Journal of Biochemical and Molecular Toxicology

WILEY

RESEARCH ARTICLE

Novel Isoindole-1,3-Dione-Isoxazole Hybrids: Synthesis, Characterization, Evaluation of Their Inhibitory Activities on Carbonic Anhydrase and Acetylcholinesterase

Özlem Gündoğdu Aytaç[1] | Hilal Başak Gündoğdu[2] | Sertan Aytaç[1] | Zeynebe Bingöl[3] | İlhami Gülçin[2] | Yunus Kara[2]

[1]Department of Food Technology, Kaman Vocational School, Ahi Evran University, Kirsehir, Turkey | [2]Department of Chemistry, Faculty of Science, Atatürk University, Erzurum, Turkey | [3]Department of Medical Services and Techniques, Tokat Vocational School of Health Services, Gaziosmanpasa University, Tokat, Türkiye

Correspondence: Özlem Gündoğdu Aytaç (ogundogdu@ahievran.edu.tr) | Yunus Kara (yukara@atauni.edu.tr)

Received: 30 May 2025 | **Revised:** 11 September 2025 | **Accepted:** 27 September 2025

Funding: The authors are appreciative to Department of Chemistry and Atatürk University for financial support.

Keywords: acetylcholinesterase | carbonic anhydrase | inhibition effects | isoindole-1,3-dione | isoxazole ring

ABSTRACT

It is known that compounds containing isoxazole units exhibit a high potential for biological activity due to the isoxazole ring. In this study, eight hexahydro-5*H*-isoxazolo[4,5-*f*]isoindole-5,7(6*H*)-dione derivatives bearing isoxazole moieties were synthesized and their inhibitory effects on various metabolic enzymes, including acetylcholinesterase (AChE) and human carbonic anhydrase isoforms I and II (hCA I and hCA II), which are associated with global disorders such as Alzheimer's disease (AD), epilepsy, and glaucoma, were investigated. Among the synthesized compounds, derivatives **9–12** exhibited notable inhibitory activity against AChE, hCA I, and hCA II enzymes. The IC_{50} values were determined to be in the ranges of 4.65–12.83 nM for AChE, 23.17–79.58 nM for hCA I, and 36.58–88.28 nM for hCA II. Molecular docking studies of the synthesized compounds **9a–12a** were carried out against three proteins: 1AZM (Human carbonic anhydrase I), 5AML (three-dimensional structure of human carbonic anhydrase II) and 4EY6 (recombinant human acetylcholinesterase). AZA and Tacrine were used as references in the docking analyses. All compounds were determined to have a higher binding affinity than Tacrine (−7.04 kcal/mol) and AZA (−6.12 and −6.24 kcal/mol). The results of inhibition tests showed that some isoxazole derivatives (**9–12**) showed significant inhibitory effects against both CA and AChE enzymes.

1 | Introduction

Heterocyclic compounds containing oxygen and nitrogen atoms are of interest as an important class of compounds in synthetic organic and medicinal chemistry due to their versatile applications. In this context, the synthesis of new heterocyclic rings from a simple molecule with different functional groups makes a significant contribution to heterocyclic chemistry.

Isoxazole (**1**) is a five-membered heterocyclic compound with oxygen and nitrogen atoms at the 1,2 positions of the ring. Its partially saturated analogues are known as isoxazolines (**2a–c**), while its fully saturated form is called isoxazolidine (**3**) (Figure 1).

Isoxazolines (**2**) are valuable intermediates that provide access to a variety of functionalized compounds such as amino alcohols,

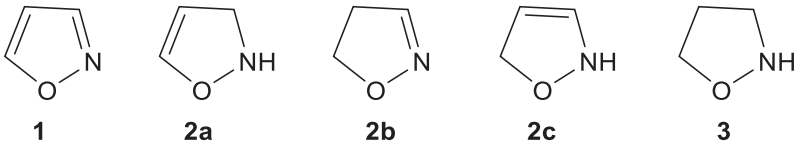

FIGURE 1 | Structures of isoxazole (**1**), isoxazolines (**2a–c**) and isoxazolidine (**3**).

hydroxy ketones, and isoxazolidines; they are essential scaffolds in the synthesis of natural products and biologically active heterocycles.

Many studies have reported the synthesis of compounds with isoxazoline-based molecules, and various biological effects of these compounds have been investigated in detail. These studies have shown that isoxazoline derivatives may have the following properties: anti-inflammatory [1], anticancer [2], antifungal [3], antibacterial [4], antioxidant [5], antiasthmatic [6, 7], antinociceptive [8], hypoglycemic [9, 10], antimalarial [11], antituberculosis [12], and antithrombotic activity [13].

Carbonic anhydrase (CA) is a family of zinc-containing metalloenzymes that catalyze the reversible hydration of carbon dioxide (CO_2) to bicarbonate (HCO_3^-) and protons (H^+). This reaction is essential for maintaining acid–base balance in various physiological systems, facilitating CO_2 transport, and regulating pH in various tissues [14, 15]. In living metabolism, there are 16 isoforms of carbonic anhydrase, each with distinct tissue distributions and functions [16, 17]. For instance, CA II is highly active and predominantly found in red blood cells, aiding rapid CO_2 transport from tissues to the lungs. CA IX and CA XII are transmembrane enzymes overexpressed in certain cancers, contributing to tumor acidification and progression.

The active site of the enzyme contains a zinc ion, which is usually coordinated by three histidine residues that are essential for catalytic activity. Inhibitors targeting specific carbonic anhydrase isoforms have been used therapeutically to treat glaucoma, epilepsy, and some cancers [18, 19].

CA inhibitors (CAIs) have been developed as diuretics, antiglaucoma, antiepileptic, and antitumor agents and continue to be important targets for both biochemical and pharmacological research [20, 21].

Among the isoforms, cytosolic CA I and CA II are the most extensively studied. CA I is mainly found in red blood cells and the gastrointestinal tract, while CA II is more widely distributed among almost all tissues [22, 23]. Notably, CA II inhibition is known to be physiologically important and has been associated with several diseases, including kidney, lung and esophageal cancers and glaucoma [24, 25]. Furthermore, CA II inhibition has been shown to suppress angiogenesis by disrupting vascular endothelial growth factor (VEGF) receptor signaling pathways [26].

Acetylcholinesterase (AChE) is another critical enzyme that hydrolyzes the neurotransmitter acetylcholine to choline and acetate, thereby terminating synaptic transmission at cholinergic synapses [27–29].

This rapid enzymatic action is essential for muscle contraction and proper neural communication. AChE is primarily located in neuromuscular junctions and cholinergic synapses in the brain [30]. Structurally, AChE contains an active site gate lined with aromatic residues, facilitating the efficient hydrolysis of acetylcholine [31].

Inhibition of AChE leads to the accumulation of acetylcholine, which results in prolonged stimulation of muscles, glands, and central nervous system receptors. This mechanism is exploited both in therapeutic applications (e.g., treatment of Alzheimer's disease and myasthenia gravis) and by certain neurotoxins [32]. AChE inhibitors such as galantamine, rivastigmine, donepezil, and tacrine are widely used in the treatment of Alzheimer's disease (AD). However, these drugs are limited by their short half-lives and adverse effects, including nausea, vomiting, and gastrointestinal disturbances. Moreover, they provide only symptomatic relief or slow the progression of the disease rather than halting it. Therefore, the development of novel AChE inhibitors with higher efficacy and improved safety profiles is crucial for achieving significant progress in AD therapy [28, 33].

Recently, we synthesized a series of substituted isoindole-1,3-dione derivatives and investigated some of their biological properties [34, 35]. Considering the various biological activities exhibited by isoxazole derivatives, we decided to design and synthesize new hybrid isoindole-1,3-dione compounds containing isoxazole moiety. We then evaluated the carbonic anhydrase and AChE enzyme inhibition activities of these synthesized compounds.

In this study, newly synthesized isoindole-1,3-dione derivatives were evaluated for their inhibitory effects on AChE, carbonic anhydrase I (hCA I), and carbonic anhydrase II (hCA II) enzymes, which are associated with global disorders such as Alzheimer's disease (AD), glaucoma, and epilepsy. The inhibitory potentials of the compounds were compared with those of clinically used standard inhibitors, namely tacrine for AChE and acetazolamide for CA isoenzymes. Furthermore, molecular docking studies were conducted to investigate the interactions between the synthesized compounds and target proteins at the molecular level. Finally, the drug-likeness and pharmacokinetic profiles of the compounds were assessed through ADME (absorption, distribution, metabolism, and excretion) analysis to determine their potential as therapeutic agents.

2 | Materials and Methods

2.1 | Chemical Part

2.1.1 | Chemical Materials and Apparatus

All chemicals were commercially available and purchased from Merck and Sigma-Aldrich. AChE, acetylcholine iodide, 5,5′-dithio*bis* (2-nitrobenzoic acid) (DTNB) and solvents were

obtained from Sigma-Aldrich (Sigma-Aldrich GmbH, Steinheim, Germany). They were analytical grade and used without further purification steps.

2.2 | Material and Apparatus

Reactions were monitored via thin-layer chromatography (TLC). Column chromatography: Silica gel 60 (70–230 mesh) and Analytical thin layer chromatography (TLC): Silica gel 60 F254. ^{1}H NMR and ^{13}C NMR spectra were recorded on 400 and 100 MHz with Varian spectrometer using $CDCl_3$. Melting points were determined on a capillary melting apparatus (BUCHI 530) and are uncorrected. HR-MS: electron spray technique (M+/M−) from the soln. in MeOH (Waters LCT Premier TM XE UPLC/MS TOF (Manchester, UK).

2.2.1 | General Procedure for Tetrahydro-1*H*-Isoindole-1,3(2*H*)-Dione Derivatives 4–7

2-Alkyl/aryl-3a,4,7,7a-tetrahydro-1*H*-isoindole-1,3(2*H*)-dione **4–7** were synthesized as described in literature [34, 36–40].

2.2.2 | General Procedure for Isoxazole Derivatives 9–12

To a solution of compound **4/7** (1 mmol) in dichloromethane (10 mL), compound **8** (1.1 mmol) and NÅCl (9%–12% in H_2O, 8 mL) were added at 0°C. Then the reaction mixture was stirred at room temperature for 16 h. The progress of the reaction was monitored by TLC analysis (40% ethyl acetate/hexanes). After completion of the reaction, the solvent was evaporated, and the residue was quenched with water (20 mL), and extracted with dichloromethane. The organic layers were combined, washed with water and brine, and dried over anhydrous Na_2SO_4. Evaporation of the solvent under high vacuum gave the compound **9a/12a** and **9b/12b**. The reaction mixture was separated by silica gel column chromatography. Total yields: 80%–85%. *syn*- and *anti*-isomers ratio: 1:3.

***Syn*−6-methyl-3-phenyl-3a,4,4a,7a,8,8a-hexahydro-5*H*-isoxazolo[4,5-*f*]isoindole-5,7(6*H*)-dione (9a):** 21% yield. Yellow viscous. ^{1}H NMR (400 MHz, $CDCl_3$) δ 7.56–7.51 (m, 2H), 7.37 (m, 3H), 4.86 (ddd, $J = 11.2$, 5.0, 2.9 Hz, 1H), 3.81 (ddd, $J = 10.9$, 6.7, 3.9 Hz, 1H), 2.93 (s, 3H), 2.52–2.44 (m, 1H), 2.23–2.10 (m, 2H), 2.07–1.95 (m, 1H). ^{13}C NMR (100 MHz, $CDCl_3$) δ 180.08, 178.69, 160.12, 130.49, 129.07, 128.58, 127.25, 78.66, 43.91, 36.75, 35.48, 24.98, 24.93, 20.86. HRMS: (ESI), m/z: Calculated for [M+H]+ $C_{16}H_{16}N_2O_3$: 285.1161; Found: 285.1237.

***Anti*−6-methyl-3-phenyl-3a,4,4a,7a,8,8a-hexahydro-5*H*-isoxazolo[4,5-*f*]isoindole-5,7(6*H*)-dione (9b):** 63% yield. White solid. Mp. 185°C–187°C. ^{1}H NMR (400 MHz, $CDCl_3$) δ 7.66–7.61 (m, 2H), 7.47–7.40 (m, 3H), 5.02 (ddd, $J = 11.1$, 4.4, 2.7 Hz, 1H), 3.93 (ddd, $J = 11.0$, 5.3, 3.7 Hz, 1H), 3.16–3.07 (m, 1H), 2.97 (s, 3H), 2.68 (ddd, $J = 12.1$, 9.4, 5.7 Hz, 1H), 2.54 (ddd, $J = 14.6$, 6.4, 4.6 Hz, 1H), 2.26 (ddd, $J = 14.3$, 5.6, 3.6 Hz, 1H), 1.89–1.78 (m, 1H), 1.72 (ddd, $J = 14.3$, 12.2, 5.5 Hz, 1H). ^{13}C NMR (100 MHz, $CDCl_3$) δ 179.58, 179.36, 157.94, 130.69, 129.33, 128.36, 127.09, 78.18, 44.37, 36.26, 34.71, 25.17, 24.59, 22.32. HRMS: (ESI), m/z: Calculated for [M+H]+ $C_{16}H_{16}N_2O_3$: 285.1161; Found: 285.1237.

***Syn*−6-ethyl-3-phenyl-3a,4,4a,7a,8,8a-hexahydro-5*H*-isoxazolo[4,5-*f*]isoindole-5,7(6*H*)-dione (10a):** 22% yield. White solid. Mp. 61°C–63°C. ^{1}H NMR (400 MHz, $CDCl_3$) δ 7.51–0.46 (m, 2H), 7.33–7.29 (m, 3H), 4.83–4.69 (m, 1H), 3.72 (ddd, $J = 11.0$, 6.9, 4.0 Hz, 1H), 3.40 (q, $J = 14.2$, 6.7 Hz, 2H), 2.86–2.77 (m, 2H), 2.43–2.34 (m, 1H), 2.15–2.03 (m, 2H), 1.98–1.90 (m, 1H), 1.11 (t, $J = 7.1$ Hz, 3H). ^{13}C NMR (100 MHz, $CDCl_3$) δ 179.50, 178.13, 159.85, 130.17, 128.83, 128.48, 126.99, 78.43, 43.59, 36.51, 35.18, 34.06 24.44, 20.42, 12.42. HRMS: (ESI), m/z: Calculated for [M+H]+ $C_{17}H_{18}N_2O_3$: 299.1317; Found: 299.1396.

***Anti*−6-ethyl-3-phenyl-3a,4,4a,7a,8,8a-hexahydro-5*H*-isoxazolo[4,5-*f*]isoindole-5,7(6*H*)-dione (10b):** 60% yield. White solid. Mp. 152°C–154°C. ^{1}H NMR (400 MHz, $CDCl_3$) δ 7.69–7.63 (m, 2H), 7.47–7.40 (m, 3H), 5.01 (ddd, $J = 11.1$, 4.6, 2.8 Hz, 1H), 3.96–3.89 (m, 1H), 3.55 (q, $J = 7.2$ Hz, 2H), 3.18–3.05 (m, 1H), 2.69 (ddd, $J = 11.7$, 9.4, 5.7 Hz, 1H), 2.52 (ddd, $J = 14.6$, 6.3, 4.8 Hz, 1H), 2.26 (ddd, $J = 14.3$, 5.6, 4.0 Hz, 1H), 1.92–1.82 (m, 1H), 1.75 (ddd, $J = 14.2$, 11.8, 5.5 Hz, 1H), 1.15 (t, $J = 7.2$ Hz, 3H). ^{13}C NMR (100 MHz, $CDCl_3$) δ 179.07, 178.89, 157.73, 130.43, 130.14, 129.09, 128.46, 128.21, 126.88, 77.93, 44.11, 36.03, 34.47, 33.74, 24.45, 22.13, 13.04. HRMS: (ESI), m/z: Calculated for [M+H]+ $C_{17}H_{18}N_2O_3$: 299.1317; Found: 299.1396.

***Syn*−3,6-diphenyl-3a,4,4a,7a,8,8a-hexahydro-5*H*-isoxazolo[4,5-*f*]isoindole-5,7(6*H*)-dione (11a):** 23% yield. White solid. Mp. 219°C–221°C. ^{1}H NMR (400 MHz, $CDCl_3$) δ 7.56–7.46 (m, 4H), 7.42–7.34 (m, 6H), 5.00 (m, 1H), 3.95–3.84 (m, 1H), 3.16 (d, $J = 2.5$ Hz, 2H), 2.77 (d, $J = 14.0$ Hz, 1H), 2.42 (d, $J = 14.8$ Hz, 1H), 2.24 (d, $J = 15.6$ Hz, 1H), 2.11–2.03 (m, 1H). ^{13}C NMR (100 MHz, $CDCl_3$) δ 179.20, 177.54, 160.63, 132.46, 130.52, 129.45, 129.10, 128.88, 128.47, 127.34, 127.08, 78.59, 77.58, 77.26, 76.94, 43.83, 36.78, 35.60, 24.95, 20.63. HRMS: (ESI), m/z: Calculated for [M+H]+ $C_{21}H_{18}N_2O_3$: 347.1317; Found: 347.1392.

***Anti*−3,6-diphenyl-3a,4,4a,7a,8,8a-hexahydro-5*H*-isoxazolo[4,5-*f*]isoindole-5,7(6*H*)-dione (11b):** 62% yield. White solid. Mp. 197°C–198°C. ^{1}H NMR (400 MHz, $CDCl_3$) δ 7.73–7.67 (m, 2H), 7.54–7.38 (m, 6H), 7.31–7.25 (m, 2H), 5.10 (ddd, $J = 11.1$, 4.4, 2.7 Hz, 1H), 4.01 (ddd, $J = 10.9$, 5.2, 4.0 Hz, 1H), 3.39–3.27 (m, 1H), 2.90 (ddd, $J = 11.9$, 9.7, 5.7 Hz, 1H), 2.64 (ddd, $J = 14.7$, 6.4, 4.7 Hz, 1H), 2.38 (ddd, $J = 14.2$, 5.6, 3.7 Hz, 1H), 2.02 (ddd, $J = 14.3$, 9.3, 3.7 Hz, 1H), 1.91 (ddd, $J = 14.2$, 12.0, 5.5 Hz, 1H). ^{13}C NMR (100 MHz, $CDCl_3$) δ 178.25, 178.06, 157.78, 131.62, 130.52, 129.23, 129.15, 128.76, 128.20, 126.92, 126.36, 77.96, 44.20, 36.23, 34.70, 24.61, 22.33. HRMS: (ESI), m/z: Calculated for [M+H]+ $C_{21}H_{18}N_2O_3$: 347.1317; Found: 347.1392.

***Syn*−6-benzyl-3-phenyl-3a,4,4a,7a,8,8a-hexahydro-5*H*-isoxazolo[4,5-*f*]isoindole-5,7(6*H*)-dione (12a):** 20% yield. White solid. Mp. 152–155 ^{1}H NMR (400 MHz, $CDCl_3$) δ 7.46–7.41 (m, 2H), 7.31–7.23 (m, 5H), 7.19–7.12 (m, 3H), 4.71 (ddd, $J = 11.1$, 5.8, 3.3 Hz, 1H), 4.51 (s, 2H), 3.65 (dt, $J = 11.4$,

5.8 Hz, 1H), 2.82–2.69 (m, 2H), 2.25 (dt, $J = 14.5$, 5.3 Hz, 1H), 2.12–2.02 (m, 1H), 1.98–1.90 (m, 2H). ^{13}C NMR (100 MHz, $CDCl_3$) δ 179.18, 177.95, 159.63, 135.71, 130.27, 129.00, 128.87, 128.55, 128.48, 127.87, 127.07, 78.52, 43.95, 42.52, 36.73, 35.33, 24.68, 20.75. HRMS: (ESI), m/z: Calculated for [M+H]+ $C_{22}H_{20}N_2O_3$: 361.1474; Found: 361.1548.

***Anti*−6-benzyl-3-phenyl-3a,4,4a,7a,8,8a-hexahydro-5*H*-isoxazolo[4,5-*f*]isoindole-5,7(6*H*)-dione (12b):** 60% yield. White solid. Mp. 84°C–86°C. ^1H NMR (400 MHz, $CDCl_3$) δ 7.67–7.59 (m, 2H), 7.46–7.40 (m, 3H), 7.38–7.24 (m, 5H), 4.94 (ddd, $J = 11.1$, 4.6, 3.0 Hz, 1H), 4.64 (s, 2H), 3.88–3.76 (m, 1H), 3.15-3.07 (m, 1H), 2.71 (ddd, $J = 11.4$, 9.5, 5.7 Hz, 1H), 2.50 (ddd, $J = 14.6$, 10.5, 5.3 Hz, 1H), 2.22 (dt, $J = 14.2$, 5.4 Hz, 1H), 1.93–1.82 (m, 1H), 1.74 (ddd, $J = 14.3$, 11.6, 5.4 Hz, 1H). ^{13}C NMR (100 MHz, $CDCl_3$) δ 178.87, 178.72, 157.74, 135.74, 130.44, 129.09, 128.73, 128.63, 128.20, 128.08, 126.88, 77.86, 44.00, 42.37, 36.12, 34.57, 24.45, 22.15. HRMS: (ESI), m/z: Calculated for [M+H]+ $C_{22}H_{20}N_2O_3$: 361.1474; Found: 361.1548.

2.3 | Biological Part

2.3.1 | AChE Inhibition Assay

The AChE inhibitory activity of isoxazole derivatives (**9–12**) was evaluated using a modified version of the Ellman's assay (1961), as described in previous studies [41]. Acetylthiocholine iodide (AChI) and 5,5′-dithio*bis* (2-nitrobenzoic acid) (DTNB) were employed as substrates for the cholinergic reaction. Briefly, 1 mL of Tris-HCl buffer (1.0 M, pH 8.0), 10 μL of varying concentrations of the isoxazole derivatives (**9–12**), and 50 μL of AChE enzyme were mixed in a test tube. The mixture was incubated at 25°C for 15 min, followed by the addition of 50 μL of DTNB solution (0.5 mM). The reaction was initiated by adding 50 μL of AChI solution (10 mM), and the absorbance was recorded at 412 nm. All experiments were performed in triplicate, and results were reported as the arithmetic mean of the three independent measurements.

2.3.2 | Purification and Activity Assay of hCA I and II Isoforms

Both hCA I and II isoforms were purified using affinity chromatography with Sepharose-4B-L-tyrosine-sulfanilamide affinity matrix as described previously [42]. The enzymatic activity of both isoforms was determined spectrophotometrically using the Verpoorte method (1967) [43]. One unit of carbonic anhydrase (CA) activity is defined as the amount of enzyme that catalyzes the conversion of p-nitrophenyl acetate to *p*-nitrophenolate at 348 nm, 25°C and within 3 min. The amount of protein was measured spectrophotometrically at 595 nm using the Bradford assay using bovine serum albumin as a standard [44]. The purity of the enzymes was assessed by SDS-PAGE according to the Laemmli method using 3% and 10% acrylamide concentrations [45]. All experiments regarding carbonic anhydrase inhibition were performed in triplicate and the results were expressed as the arithmetic mean of three independent measurements.

2.3.3 | IC_{50} Values Determination

IC_{50} values were determined from the plots of enzyme activity (%) versus concentrations of synthesized compounds [46]. Ki values and other inhibition parameters were obtained using Lineweaver–Burk plots (1934) [47].

2.4 | Molecular Docking Studies

Molecular docking calculations are often performed to support experimental studies and identify active sites in molecules. Molecular modeling is an important approach used to study protein-ligand interactions, and these interactions are detailed through molecular docking analyses. This method allows for the assessment of potential biological activities and binding patterns of molecules toward proteins. An increase in the resulting interaction level indicates an increase in the biological activity of the molecule. Various parameters are obtained from the calculations, and each of these parameters provides information about different properties of the molecules. When these parameters are examined, the docking score is the primary criterion for determining the activity of molecules [29].

Molecular docking provides valuable information about the activity and safety of compounds in drug design and development [48]. Therefore, in this study, molecular docking analyses were performed by selecting molecules **9a–12a** using Tacrine and AZA as reference compounds. The molecular structures of the target compounds were designed and optimized using ChemDraw 19.0. These structures were then converted into three-dimensional (3D) molecular models and saved in PDB (Protein Data Bank) format using Avogadro, thus enabling proper geometry optimization and energy minimization.

According to the experimental procedure and literature, target proteins were selected as hCAI/PDB: 1AZM [49, 50], hCAII/PDB: 5AML [51, 52] and AChE/PDB: 4EY6 [53, 54] and 3D-pdb versions of the receptors were retrieved from the protein database (https://www.rcsb.org/). Virtual screening and molecular docking studies were conducted using 5-acetamido-1,3,4-thiadiazole-2-sulfonamide as a template for hCA I, 2-(but-2-yn-1-ylsulfamoyl)−4-sulfamoylbenzoic acid as a template for hCA II, and galantamine, an AChE inhibitor, as a template. By analyzing the compatibility of candidate molecules with template structures, this method enabled the identification of compounds with high binding potential for target proteins [29].

Before molecular docking, ligands and protein structures were prepared using AutoDock Tools 1.5.7. This process included removing water molecules, adding polar hydrogen atoms, and determining appropriate docking parameters. Both ligand and protein molecules were then converted to the PDBQT file format, which is required for docking simulations in AutoDock. Molecular docking was performed to predict the binding affinity and the mode of interaction between the ligands and the active sites of the proteins. The grid parameters were selected with $60 \times 60 \times 60$ Å; x, y, z dimensions and a spacing of 0.553 Å. The center of the complex formed by Human Carbonic Anhydrase I (PDB: 1AZM) was determined as x: 34.854, y: 16.460, z: −18.545. Similarly, the center coordinates for the three-dimensional structure of Human

Carbonic Anhydrase II (PDB: 5AML) were identified as x: −4.711, y: 3.797, z: 14.303. Additionally, the center of the complex formed by Recombinant Human Acetylcholinesterase (PDB: 4EY6) was determined as x: −9.942, y: −43.488, z: 30.291. The resulting protein-ligand complexes were analyzed using BioVia Discovery Studio Software, which allows visualization of hydrogen bond interactions, hydrophobic contacts, π–π stacking, and other non-covalent interactions critical for binding stability.

2.5 | ADME Prediction Results

Computer-aided ADMET predictions play a crucial role in assessing a compound's suitability for drug development and enhancing the efficiency and cost-effectiveness of the drug discovery process. In this study, ADMETlab 2.0, a web-based tool for evaluating ADMET characteristics [55], was utilized to analyze the ADMET profiles of all compounds.

The molecular properties of compounds **5a–d**, including their human oral absorption rates and similarities to known drugs, were predicted using SwissADME [56]. Various factors are examined to determine the potential efficacy, safety, and bi-availability of a chemical, and predicting how the compound behaves in the body is critical in drug research. All these factors contribute to the molecular and ADME properties of a compound, which in turn guides its optimization as a potential drug. Ideal drug candidates provide adequate bi-availability, efficacy, safety, and manufacturability [57].

3 | Result and Discussion

3.1 | Chemistry Part

The use of various modifications of the isoxazole unit in the synthesis of some natural products and biologically active molecules has led researchers to develop various synthetic approaches for the synthesis of isoxazole ring systems [58–60]. One of these methods involves one-pot addition of oxime compounds to appropriate double bonds in dichloromethane (CH_2Cl_2) in the presence of sodium hypochlorite (NaOCl) [61, 62]. In particular, we preferred this method because it is a cheap, one-pot and easily applicable synthesis method. We aimed to synthesize hybrid isoindole-1,3-dione derivatives containing a novel isoxazole unit using this strategy. For this purpose, isoindole-1,3-dione derivatives **4–7** synthesized in previous studies were used as starting materials (Scheme 1) [34, 36–40].

Following the synthesis of isoindole-1,3-dione derivatives, their reactions with oxime compounds were investigated. Benzaldehyde oxime, used for the construction of the isoxazole ring, was synthesized according to a method previously reported in the literature. This oxime was then reacted with the isoindole-1,3-dione derivatives in the presence of sodium hypochlorite (NaOCl) in dichloromethane (CH_2Cl_2) at room temperature (Scheme 2).

Considering the structure of the bicyclic imide molecule, it can lead to the formation of *syn*- and *anti*-isomers by 1,3-dipolar cycloaddition reaction. The ^{1}H NMR spectrum recorded of the crude reaction mixture confirmed the occurrence of the addition reaction and revealed that the *syn*- and *anti*-isomers were in the ratio of 1:3. Due to the steric effect, it was predicted that the *anti*-isomer with less steric hindrance would be the main product. The isomeric mixture was then purified and both isomers were characterized by detailed spectroscopic analysis. In this context, when we compare the NMR spectra of the *syn*- and *anti*-products, it was seen that the splitting of signal groups in the *anti*-product was more pronounced, which is consistent with its proposed configuration (Figure 2). This difference is due to the changing chemical environments of the protons in the two isomers. In

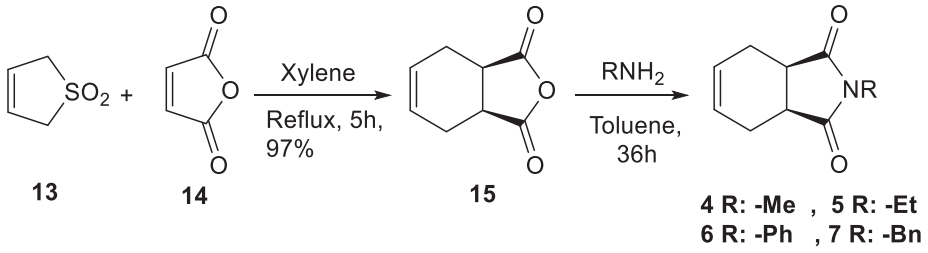

SCHEME 1 | Synthesis of tetrahydro-1*H*-isoindole-1,3(2*H*)-dione derivatives (**4–7**).

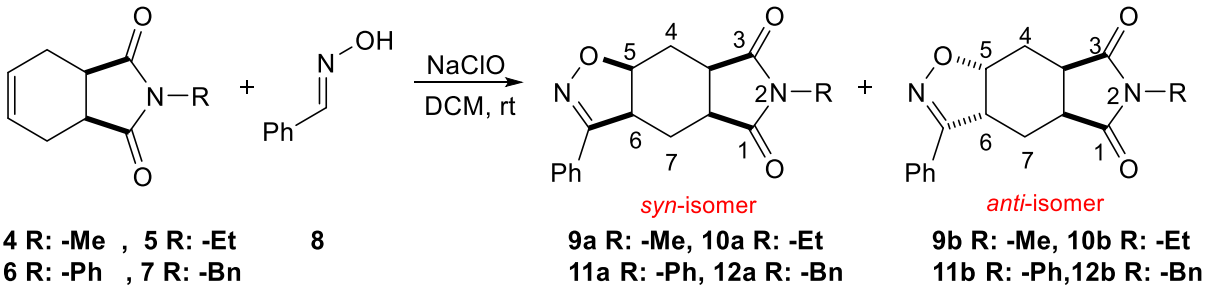

SCHEME 2 | Synthesis of hexahydro-5*H*-isoxazolo[4,5-*f*]isoindole-5,7(6*H*)-dione derivatives (**9–12**).

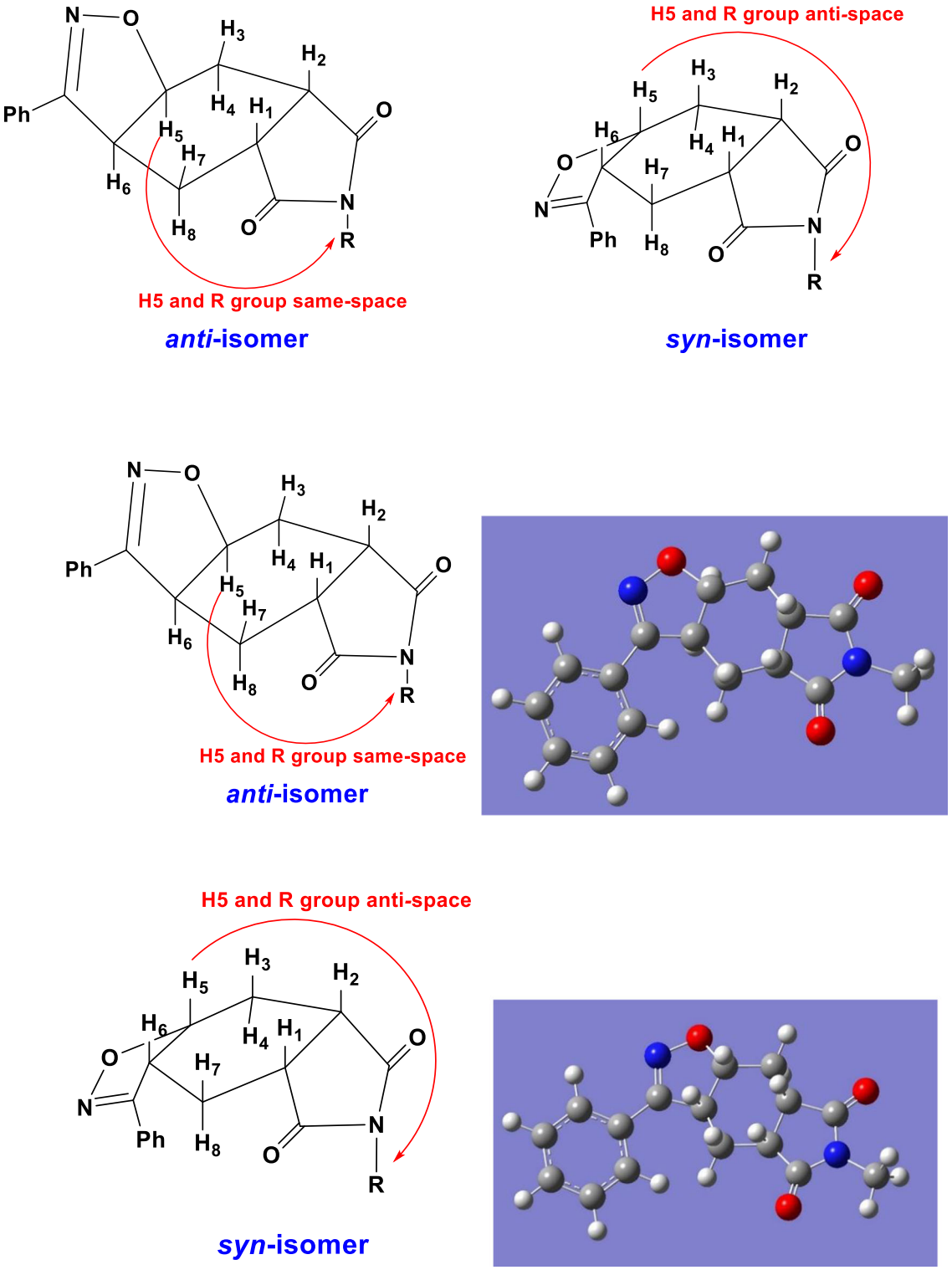

FIGURE 2 | *syn*- and *anti*-isoxazole derivatives.

the *anti*-isomer, the different chemical environments of the protons affect the proton–proton splitting more, which makes the signal splitting more pronounced. However, additional NMR experiments were required to precisely determine the stereochemistry of each isomer. One such technique is the Nuclear Overhauser Effect (NOE) experiment, which provides spatial information on proton affinity. The exact configuration of *syn*-isomer **9a** was confirmed by differential ^{1}H NMR-NOE measurements (Figure S1, p. 10).

According to the structure of compound **9a**, irradiation of the H5 proton at the common bridgehead carbon of isoxazole and the six-membered ring formed after the addition of the oxime will provide important information about the structure of the product formed. Thus, it will be determined whether the structure is in *syn*- or *anti*-configuration.

As can be seen from the NOE spectrum of compound **9a**, irradiation of the H5 proton signal ($\delta = 4.80$) caused an increase

in the signal intensities of the protons in cis configuration (i.e., H1, H2, H3, and H7) and resonated at δ = 3.81, 2.47, and 2.23 ppm, respectively. In contrast, the NOE spectrum of compound **9a** did not show a positive interaction (i.e., an increase in signal intensity) with the methyl protons attached to the nitrogen atom (δ = 2.93) when the H5 proton was irradiated. This suggests that the methyl protons and the H5 proton do not share the same space, indicating that the imide ring and the isoxazole ring are not in a *syn*-configuration. As a result, the structure of the 1,3-dipolar cycloaddition products was identified based on their spectral analysis and, as expected, the *anti*-product was found to be more formed. The synthesized isoindole-1,3-dione analogs containing isoxazole units were characterized using ^{1}H NMR, ^{13}C NMR and mass spectrometry (MS). Then, the AChE and carbonic anhydrase inhibitory activities of hybrid isoxazole derivatives were evaluated.

3.2 | Biological Part

Human carbonic anhydrase isozymes I (hCA I) and II (hCA II) play critical roles in regulating acid–base balance and are important therapeutic targets in the treatment of cerebral edema, glaucoma, and epilepsy [63, 64]. Isoxazole derivatives (9–12) demonstrated in vitro inhibitory activity against cytosolic hCA I, which is associated with cerebral and retinal edema, as well as gastric and duodenal ulcers [65, 66]. They also showed inhibition of hCA II, which is implicated in edema, glaucoma, epilepsy, and altitude (mountain) sickness [67]. In addition, these derivatives exhibited inhibitory activity against AChE, a key enzyme linked to Alzheimer's disease (AD).

The carbonic anhydrase inhibitory effects of isoxazole derivatives (9–12) were evaluated using the esterase assay and compared with the reference drug acetazolamide (AZA). To determine the activity of the synthesized isoxazole derivatives (9–12) against AChE, Ellman's procedure (1961) [68, 69] was used and compared with the standard inhibitor Tacrine. Further information on the enzyme inhibition results is presented in Tables 1 and 2.

Isoxazole derivatives (9–12) exhibited effective inhibition profiles against widespread cytosolic hCA I isozyme, with K_i values ranging of 23.17 ± 6.55 nM and 79.58 ± 13.99 nM. Compound 9a showed a lower inhibition profile (K_i: 79.58 ± 13.99 nM) compared to the synthesized isoxazole derivatives. However, in this series, compound 11a was found to be the most potent inhibitor of cytosolic hCA I isozyme (K_i: 23.17 ± 6.55 nM) compared to AZA (K_i: 19.41 ± 3.41 nM).

Isoxazole derivatives (9–12) inhibited cytosolic and predominant human carbonic anhydrase II (hCA II) isoenzyme with

TABLE 1 | The summarized inhibition parameters of synthesized isoxazole derivatives (9–12) toward human carbonic anhydrase I and II isoform (hCA I and II) and AChE.

	IC_{50} (nM)						K_I (nM)		
Compounds	**hCA I**	r^2	**hCA II**	r^2	**AChE**	r^2	**hCA I**	**hCA II**	**AChE**
9a	53.31	0.9808	43.31	0.9744	8.88	0.9814	79.58 ± 13.99	42.60 ± 10.03	1.85 ± 0.18
9b	63.00	0.9748	49.54	0.9832	7.70	0.9919	60.63 ± 12.64	41.22 ± 8.84	1.89 ± 0.04
10a	43.31	0.9912	69.30	0.9910	12.83	0.9630	31.10 ± 3.14	36.58 ± 6.67	1.94 ± 0.53
10b	42.52	0.9771	67.28	0.9717	10.19	0.9744	48.31 ± 5.70	88.28 ± 10.22	1.48 ± 0.16
11a	26.65	0.9716	49.15	0.9944	4.65	0.9964	23.17 ± 6.55	37.05 ± 10.55	2.51 ± 0.42
11b	49.50	0.9705	66.63	0.9719	11.95	0.9777	28.52 ± 10.85	67.07 ± 8.93	3.73 ± 0.84
12a	46.200	0.9893	38.500	0.9801	7.37	0.9736	37.45 ± 9.85	75.81 ± 11.46	4.02 ± 0.88
12b	33.00	0.9807	46.20	0.9823	5.50	0.9778	31.45 ± 8.50	40.17 ± 5.11	1.99 ± 0.33
AZA	38.500	0.9868	49.500	0.9852	—	—	19.41 ± 3.41	44.60 ± 10.45	—
Tacrine	—	—	—	—	7.14	0.9788	—	—	2.82 ± 0.77

TABLE 2 | Docking score (Kcal/Mol).

Compounds	**1AZM (human carbonic anhydrase I)**	**5AML (human carbonic anhydrase II)**	**4EY6 (human acetylcholinesterase)**
AZA	−6.12	−6.24	—
9a	−6.9	−6.86	−8.99
10a	−6.75	−6.82	−9.18
11a	−7.62	−7.31	−9.58
12a	−7.40	−7.25	−10.49
Tacrine	—	—	−7.04

Ki's of 36.58 ± 6.67–88.28 ± 10.22 nM. Among them, compound 10a showed the strongest inhibitory effect against hCA II with Ki's of 36.58 ± 6.67 nM. Also, compounds 9a, 9b, 11a, 12b showed remarkable inhibitory effects against hCA II with Ki's of 41.22 ± 8.84, 42.60 ± 10.03, 37.05 ± 10.55, 40.17 ± 5.11 nM, respectively. In contrast, compounds 10b, 11b, and 12a showed lower inhibitory activity compared to the reference compound acetazolamide (AZA) with a Ki value of 44.60 ± 10.45 nM. In general, most of the synthesized isoxazole derivatives showed strong inhibitory potential against the widely expressed hCA II isoenzyme.

The AChE inhibition abilities of isoxazole derivatives (9–12) were given for the first time in this study. The results were presented and summarized in Table 1. Tacrine was used as positive control for AChE inhibition with Ki of 2.82 ± 0.77 nM against AChE enzyme. As presented in Table 1, IC_{50} values of all isoxazole derivatives (9–12) were in the range of 4.65 to 12.83 nM against AChE. Inhibition results showed that the synthesized isoxazole derivatives 11a and 12b had higher inhibitory effects than TAC (IC_{50}: 7.14 nM). 9a–b showed moderate effect inhibition, while 12a showed inhibitory activity similar to Tacrine. Isoxazole compounds 10a, 10b, and 11b showed lower inhibitory effects than Tacrine (IC_{50}: 7.14 nM).

3.3 | Molecular Dockıng Results

Molecular docking is widely recognized as a critical tool in drug design due to its ability to simulate interactions between proteins and small molecules (ligands), enabling the formation of biologically functional and stable complexes [70]. This method allows for a detailed examination of interactions between molecules and proteins, and it has been observed that as the interaction density increases, the biological activity of the molecules also rises. During molecular docking calculations, understanding how molecules bind to proteins is of great importance; this binding should occur in accordance with the classical lock-and-key model [29, 70].

Inhibition occurs as a result of interactions between proteins and molecules, and the intensity of these interactions directly affects the activity of the molecules. These interactions are generally chemical in nature, encompassing hydrogen bonds, polar and hydrophobic interactions, as well as π–π interactions. In this context, the interactions between a molecule and a protein emerge as the most critical factors determining biological activity [71]. An increase in interactions leads to enhanced molecular activities. Studies have shown that hydrogen bonds, polar and hydrophobic interactions, as well as π–π interactions, play a significant role in the interactions between molecules and proteins [70].

In this study, three proteins, **1AZM** (Human carbonic anhydrase I), **5AML** (three-dimensional structure of human carbonic anhydrase II), and **4EY6** (recombinant human AChE), were used to perform docking analyses with the synthesized compounds **9a–12a** and the reference drugs (AZA and Tacrine). Due to the structure of the *anti*- and *syn*-isomers, they may exhibit differences in terms of protein binding. However, considering the binding regions in both isomers, the *syn*- or *anti*-nature of the structure does not affect binding in terms of structure, so similar binding values were observed in preliminary experiments conducted on both isomers. Therefore, *syn*-isomers, which generally exhibit the highest biological activity, were considered in activity studies. Visualized representations of these interactions are presented in Figures 1 and 2.

When the interactions between **AZA** and **1AZM** protein were examined, conventional hydrogen bonds were observed with amino acids TRP5 (1.90 Å), ASP8 (2.03 and 3.05 Å), GLN242 (2.84 Å) and HIS243 (2.19 Å). A carbon–hydrogen bond was observed with HIS 243 (2.93 Å), a π-donor interaction was noted with TYR7 (2.44 Å). π–π T-shaped interaction was observed with TYR7 (5.53 Å). π-sulfur interactions were also observed with TYR7 (5.02 Å) and HIS64 (5.45 Å). Van der Waals interactions were identified with MET241, PRO240, SER231, ASN11, ASP4, GLY6, and GLY63. All interactions are shown in Figure 3.

When the interactions between **9a** and the 1AZM protein were examined, conventional hydrogen bonds were observed between the oxazole ring and TYR7 (2.09 Å) and ASN11 (2.39 Å). Carbon–hydrogen bonds were identified between the imide ring and SER231 (3.38 Å) and GLY6 (3.21 Å). In addition, van der Waals interactions were detected with LYS170, GLY63, HIS64, PRO240, GLN242, HIS243, MET241, ASN244, ASP8, and TRP5 residues. All these interactions are illustrated in Figure 3.

When the interactions between **10a** and the 1AZM protein were examined, a conventional hydrogen bond was observed between the imide ring and TRP5 (2.31 Å). A carbon–hydrogen bond was also observed between the imide ring and TRP5 (2.70 Å), while a π–donor hydrogen bond was established between the phenyl group and SER231 (2.44 Å). Furthermore, a π–anion interaction was detected between the phenyl group and ASP8 (4.84 Å), and π–alkyl interactions were observed between the cyclohexane ring and HIS64 (4.91 Å) and TRP5 (4.98 Å). Van der Waals interactions were identified with LYS170, GLY63, VAL239, PRO240, GLN242, MET241, HIS243, TYR7, GLY6, PRO3, ASN11, and ASP4 residues. All these interactions are illustrated in Figure 3.

When the interactions between **11a** and the 1AZM protein were examined, a conventional hydrogen bond was identified between the oxazole ring of 11a and GLN92 (1.96 Å). A carbon–hydrogen bond was observed between the oxazole ring and HIS67 (2.93 Å), and a π–donor hydrogen bond was established between the phenyl group and THR199 (2.75 Å). A π–cation interaction was detected between the phenyl group and HIS64 (4.28 Å), while a π–π T-shaped interaction was observed between the phenyl group and HIS64 (4.80 Å). π–alkyl interactions were found between the phenyl group and VAL62 (5.29 Å), between the cyclohexane ring and HIS200 (5.50 Å), and between the phenyl group in the imide ring and LEU198 (5.12 Å). Van der Waals interactions were identified with PHE91, ALA121, LEU141, VAL207, VAL143, HIS94, TRP209, HIS119, HIS96, and TRP5 residues. All these interactions are illustrated in Figure 3.

When the interactions between **12a** and the 1AZM protein were examined, a conventional hydrogen bond was observed between the imide ring and GLN92 (2.78 Å). A π–donor

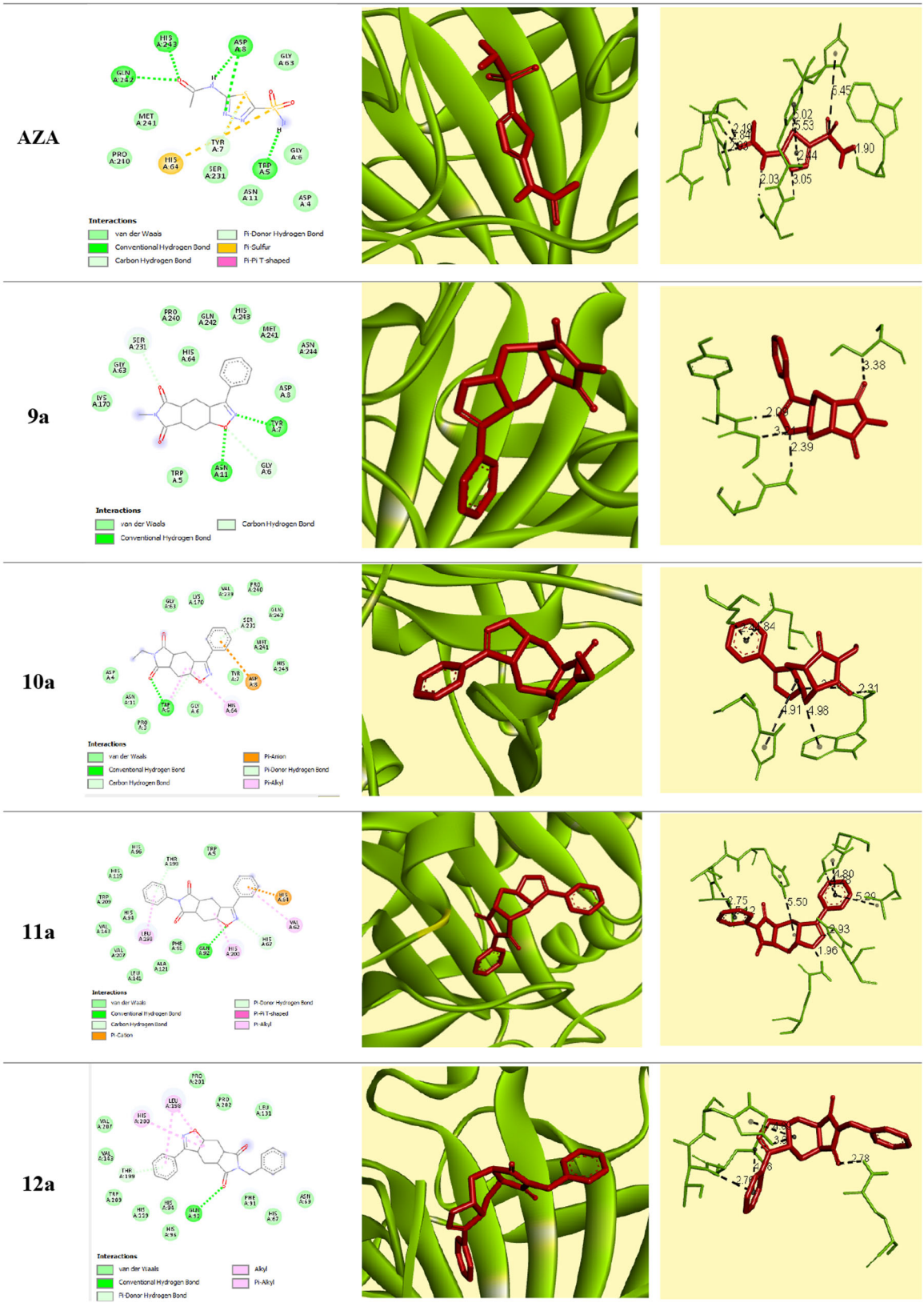

FIGURE 3 | 2D and 3D Interaction diagrams of **AZA** and compounds **9a–12a** in complex with **hCA-I** (PDB ID: **1AZM**).

hydrogen bond was detected between the phenyl group and THR199 (2.76 Å). In addition, an alkyl interaction was observed between the phenyl and cyclohexane ring and LEU198 (3.94 Å), while π–alkyl interactions were identified between the cyclohexane ring and LEU198 (4.98 Å) and HIS200 (4.89 Å). Van der Waals interactions were detected with PRO201, PRO202, LEU131, ASN69, HIS67, PHE91, HIS96, HIS94, HIS119, TRP209, VAL143, and VAL207 residues. All these

interactions are illustrated in Figure 3. The numerical values of all calculated parameters are presented in Table 2.

When the interactions between compound **AZA** and **5AML** protein were examined, conventional hydrogen bonds were observed between with the amino acids THR199 (1.84 Å), GLN92 (2.80 Å), ASN67 (1.73, 2.32, and 2.18 Å). A π-donor interaction was detected with HIS94 (3.32 Å), a π-cation interaction was observed with HIS94 (3.36 Å). π-π shaped interaction was found involving HIS94 (3.73 Å), π-sulfur interaction was observed with HIS96 (4.69 Å) amino acids. Van der Waals interactions were detected with HIS119, THR200, ASN62, ALA65, HIS64, VAL121, VAL143, LEU198, TRP209. All interactions are shown in Figure 4.

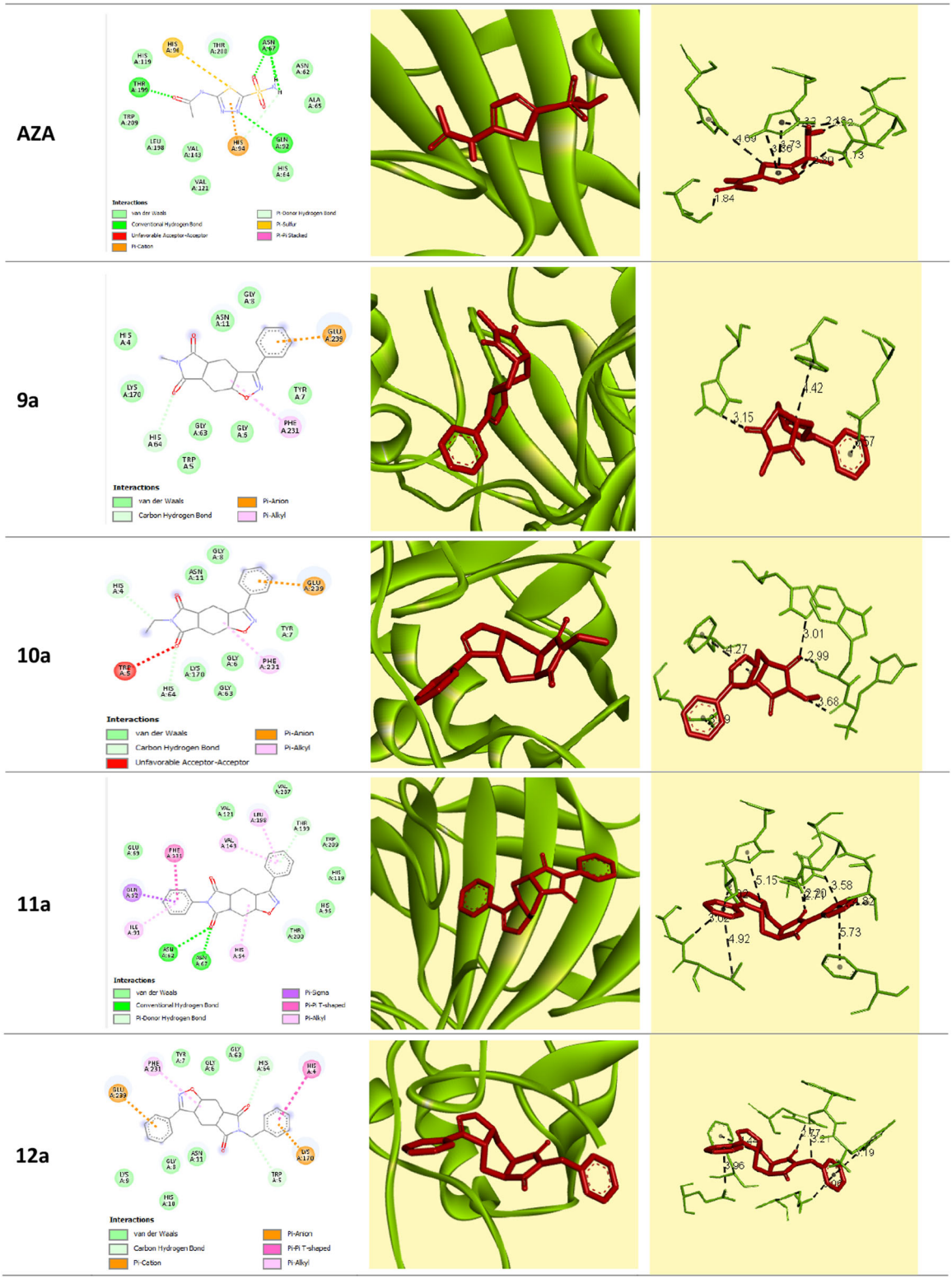

FIGURE 4 | 2D and 3D Interaction diagrams of **AZA** and compounds **9a–12a** in complex with **hCA-II** (PDB ID: **5AML**).

When the interactions between **9a** and the **5AML** protein were examined, a carbon–hydrogen bond was observed between the imide ring and HIS64 (3.15 Å). A π–anion interaction was detected between the phenyl group and GLU239 (3.57 Å), while a π–alkyl interaction was observed between the cyclohexane ring and PHE231 (4.42 Å). Furthermore, Van der Waals interactions were identified with GLY8, TYR7, GLY6, GLY63, TRP5, LYS170, HIS4, and ASN11 residues. All these interactions are illustrated in Figure 4.

When the interactions between **10a** and the **5AML** protein were examined, carbon–hydrogen bonds were identified between the imide ring and HIS4 (3.68 Å), TRP5 (2.99 Å), and HIS64 (3.01 Å). A π–anion interaction was detected between the phenyl group and GLU239 (3.69 Å), while π–alkyl interactions were observed between the cyclohexane group and PHE231 (4.27 Å) as well as TRP5 (2.99 Å). Van der Waals interactions were found with ASN11, GLY8, TYR7, GLY6, GLY63, LYS170, and HIS64 residues. All these interactions are illustrated in Figure 4.

When the interactions between **11a** and the **5AML** protein were examined, conventional hydrogen bonds were observed between the imide ring and ASN67 (2.20 Å) and ASN62 (2.71 Å). A π–donor hydrogen bond was detected between the phenyl group and THR199 (3.02 Å). A π–π T-shaped interaction was identified between the phenyl group in the imide ring and PHE131 (5.73 Å), while a π–sigma interaction was observed between the phenyl group in the imide ring and GLN92 (3.58 Å). π–alkyl interactions were found between the phenyl group of 11a and VAL143 (5.02 Å) and LEU198 (4.92 Å), between the cyclohexane group of 11a and HIS94 (5.15 Å), and between the phenyl group in the imide ring and ILE91 (4.82 Å). Van der Waals interactions were identified with GLU69, VAL121, VAL207, TRP209, HIS119, HIS96, and THR200 residues. All these interactions are illustrated in Figure 4.

When the interactions between compound **12a** and the 5AML protein were examined, carbon–hydrogen bonds were observed between the imide and benzyl groups and TRP5 (3.21 Å) and HIS64 (2.77 Å). A π–cation interaction was identified between the phenyl group in the imide ring and LYS170 (3.06 Å). A π–anion interaction was detected between the phenyl group in the oxazole ring and GLU239 (3.96 Å), and a π–π T-shaped interaction was observed between the phenyl group in the imide ring and HIS4 (5.19 Å). A π–alkyl interaction was found between the cyclohexane ring and PHE231 (4.44 Å). Additionally, Van der Waals interactions were observed with TYR7, GLY6, GLY63, ASN11, GLY8, HIS10, and LYS9 residues. All these interactions are illustrated in Figure 4.

When the interactions between **Tacrine** and **4EY6** protein were examined, conventional hydrogen bonds were observed between with the amino acids SER293 (1.89 Å) and ARG296 (1.76 Å). π–π stacked interaction was detected with TRP286 (4.76, 3.98 and 5.55 Å) and a π-alkyl interaction was observed with TRP286 (4.90 Å). Van der Waals interactions were identified with GLU292, LEU289, VAL294, PHE338, PHE295, PHE297, and TYR341. All interactions are shown in Figure 5.

When the interactions between compound **9a** and **4EY6** protein were examined, a conventional hydrogen bond was identified between the imide ring and SER293 (1.99 Å). In addition, a carbon–hydrogen bond was observed between the oxazole ring and SER293 (2.57 Å). A π–π stacked interaction was detected between the phenyl group of the imide ring and TYR341 (4.65 Å), while a π–alkyl interaction was observed between the cyclohexane group of 9a and TRP286 (4.22 Å). Furthermore, Van der Waals interactions were identified with TYR124, TYR337, PHE338, PHE297, PHE295, VAL294, ARG296, LEU289, GLN291, and GLU292 residues. All these interactions are illustrated in Figure 5.

When the interactions between compound **10a** and the 4EY6 protein were examined, a conventional hydrogen bond was identified between the imide ring and SER293 (1.98 Å). In addition, a carbon–hydrogen bond was observed between the oxazole ring and SER293 (2.54 Å). The phenyl group of the oxazole ring formed a π–π stacked interaction with TYR341 (4.68 Å), while the cyclohexane ring exhibited a π–alkyl interaction with TRP286 (4.22 Å). Furthermore, Van der Waals interactions were identified with VAL365, GLY342, VAL294, PHE297, TYR124, TYR337, PHE338, PHE295, ARG296, LEU289, GLN291, and GLU292 residues. All these interactions are illustrated in Figure 5.

When the interactions between compound **11a** and the 4EY6 protein were examined, a π–donor hydrogen bond was identified between the phenyl group attached to the imide ring and TYR124 (2.65 Å). In addition, π–π T-shaped interactions were detected between the same phenyl group and TYR124 (5.85 Å) as well as TYR341 (4.76 Å). The cyclohexane group of the molecule exhibited π–alkyl interactions with PHE338 (5.35 Å) and HIS447 (5.24 Å). Furthermore, Van der Waals interactions were identified with LEU130, ALA127, TYR119, TRP86, TYR133, TYR337, PHE295, TRP286, PHE297, GLY122, SER203, GLY121, GLU202, SER125, GLY120, and GLY126 residues. All these interactions are illustrated in Figure 5.

When the interactions of compound **12a** with 4EY6 protein were examined, a conventional hydrogen bond was detected between the oxazole ring and TYR337 (1.89 Å). In addition, π–π stacked interactions were observed between the phenyl group on the oxazole ring and TYR341 (5.03 Å). The benzyl group attached to the imide ring was found to form π–π T-shaped interactions with the amino acids HIS447 (4.76 Å), TRP86 (4.74 and 4.46 Å), and TYR337 (4.93 Å). In addition, the phenyl group on the oxazole ring was observed to form π–alkyl interactions with VAL294 (5.37 Å) and the cyclohexane ring with TYR124 (4.96 Å). Van der Waals interactions were determined with the amino acids SER125, GLY121, TYR449, GLY448, GLU202, SER203, GLY122, TRP286, PHE338, PHE297, ARG296, and PHE295. All these interactions are shown in Figure 5.

The docking score, a key measure of molecular functionality reflecting binding affinity, was calculated for the **1AZM** (Human carbonic anhydrase I), **5AML** (Human carbonic anhydrase II), **4EY6** (Human AChE) proteins, respectively. This comparison is based on the numerical values of the docking scores, with the most negative value indicating the highest activity. **AZA** exhibits binding energies of −6.12 and −6.24 kcal/mol against human carbonic anhydrase I (hCA I) and carbonic anhydrase II (hCA II) isoenzymes, respectively. In contrast, all derivatives **9a–12a** demonstrate stronger binding affinities

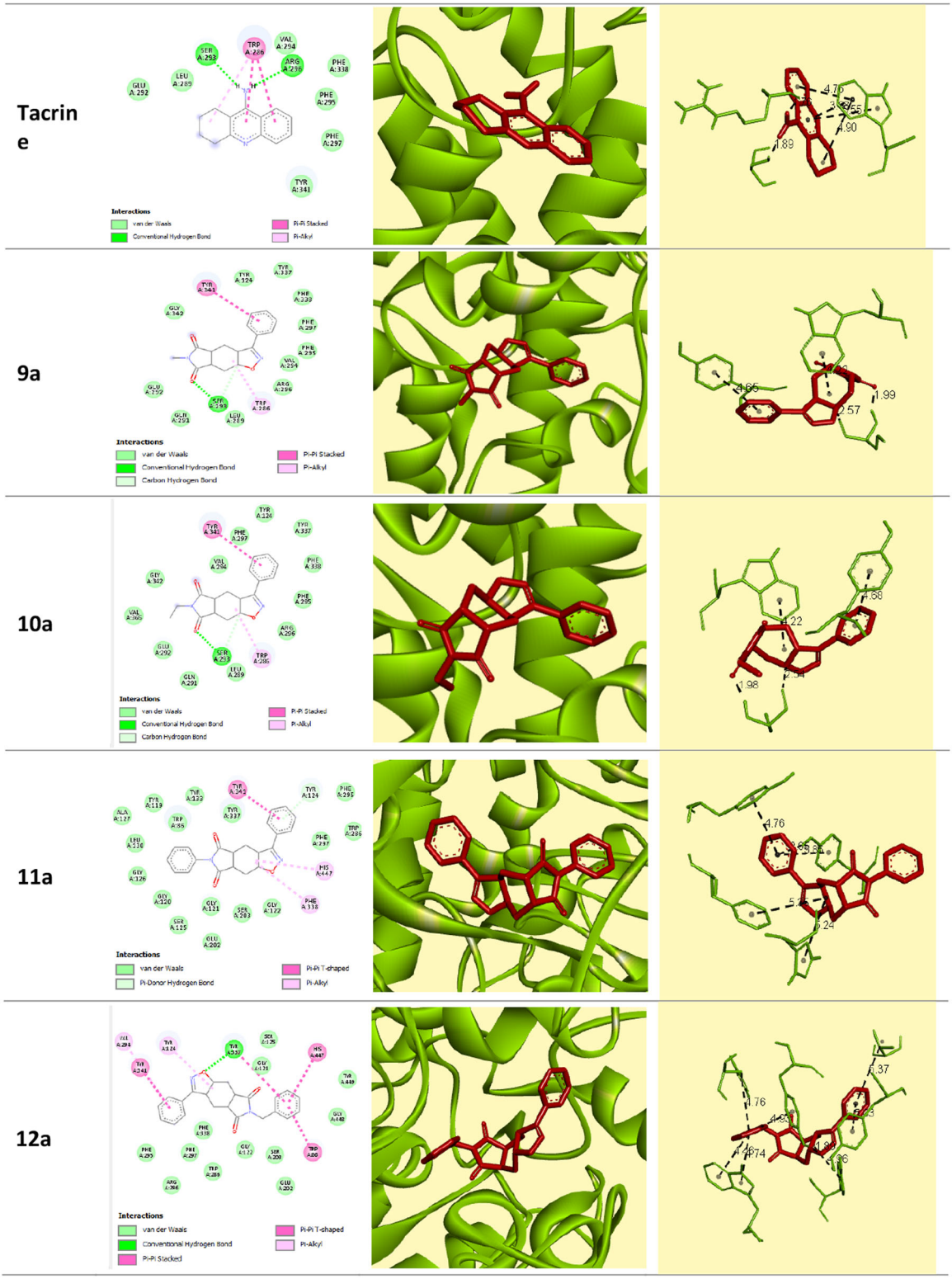

FIGURE 5 | 2D and 3D interaction diagrams of **Tacrine** and compounds **9a**–**12a** in complex with Acetylcholinesterase (PDB ID: 4EY6).

(more negative energy values) toward both enzymes (Table 2). This indicates that the synthesized derivatives possess higher affinity compared to the reference compound and may serve as more potent inhibitor candidates.

Among these, the strongest binding energy with hCA I (1AZM) is observed for compound **11a**. The binding affinity ranking against hCA I is as follows: **11a** (−7.62) > **12a** (−7.40) > **9a** (−6.90) > **10a** (−6.75) > **AZA** (−6.12) kcal/mol. Compounds **9a** and **10a** form more stable complexes than AZA, indicating higher binding affinity. Compounds **11a** and **12a** exhibit particularly strong binding energies with carbonic anhydrase I, suggesting high inhibitory potential against this target.

Similarly, compound **11a** shows the highest affinity for hCA II (5AML), with the binding energy ranking: **11a** (−7.31) > **12a** (−7.25) > **9a** (−6.86) > **10a** (−6.82) > **AZA** (−6.24) kcal/mol. Both **11a** and **12a** demonstrate the strongest binding energies toward carbonic anhydrase II, indicating a high potential to inhibit both isoenzymes, thus acting as dual inhibitors.

Importantly, all derivatives **9a–12a** exhibit significantly strong binding energies against AChE. The binding affinity order is: **12a** (−10.49) > **11a** (−9.58) > **10a** (−9.18) > **9a** (−8.99) > **Tacrine** (−7.04) kcal/mol. This suggests that especially compound **12a** has a high potential as an AChE inhibitor. Moreover, **11a** and **12a** can strongly inhibit AChE, indicating their relevance as candidates targeting enzymes involved in neurological disorders.

In summary, compounds **9a-12a** outperform the reference compounds **AZA** and **Tacrine** in terms of binding energies against carbonic anhydrase isoenzymes I and II as well as AChE. Among them, **11a** and **12a** show the highest overall binding scores, positioning them as lead candidates. Particularly, **12a** stands out as a selective AChE inhibitor due to its strongest binding affinity for this enzyme. Therefore, these compounds warrant further investigation for their enzyme selectivity and multi-target inhibitory potential in future studies.

3.4 | ADME Results

For a compound to be considered a drug candidate, it must not only exhibit potent pharmacological activity but also possess favorable properties in terms of absorption, distribution, metabolism, and excretion (ADME) parameters and comply with Lipinski's Rule of Five [72, 73]. In this context, the drug-like properties of the isoindole derivative compounds included in the study were comprehensively analyzed using the SwissADME tool. Structural parameters such as molecular weight, polar surface area, number of rotary bonds, aromaticity, and Csp^3 ratio directly affect the compounds' permeation through biological membranes, solubility, and potential interaction with target proteins. The obtained evaluation results are summarized in Table 3.

Analyzing the physicochemical and pharmacokinetic profiles of candidate molecules is critical for bioavailability, efficacy, and safety [74]. Compounds **9–12** evaluated in this study were extensively studied with respect to pharmaceutical and physicochemical parameters that are critical for drug design.

Drug-likeness refers to the likelihood of a molecule being suitable for oral administration based on its bioavailability [56], and ADME properties are closely related to the physicochemical profile of the compound. The molecular weights of compounds **9–12** range from 284.31 to 360.41 g/mol, which are in compliance with Lipinski's Rule of Five. When the fraction of Csp^3 carbon atoms is considered, higher values were observed in compounds **9a/9b** and **10a/10b** (44% and 47%, respectively), whereas lower values were noted in **11a/11b** and **12a/12b** (29% and 32%, respectively). A lower Csp^3 ratio indicates a more planar and rigid molecular structure, which may facilitate aromatic interactions such as π–π stacking with target proteins.

The total polar surface area (TPSA) was calculated as 58.97 $Å^2$ for all compounds. Since a TPSA below 140 $Å^2$ is considered favorable for good oral bioavailability, these compounds fall within an appropriate range [75]. Additionally, all compounds contain four hydrogen bond acceptor groups but lack hydrogen bond donor groups. This structural feature may facilitate passive diffusion across cellular membranes, offering a potential advantage for membrane permeability.

Lipophilicity is a key parameter that directly influences the lipid–water balance, membrane permeability, and pharmacokinetic behavior of compounds [76]. The LogP values of all compounds were found to be below 5, in accordance with Lipinski's criteria, indicating favorable membrane permeability. The average (consensus) LogP values were calculated to be approximately ~1.55 for **9a/9b**, 1.89 for **10a/10b**, 2.81 for **11a/11b**, and between 2.85 and 2.87 for **12a/12b**. This gradual increase corresponds to the rising degree of aromaticity and hydrophobic character within the compound series, as expected. A moderate level of lipophilicity (LogP between 1 and 3) is considered beneficial for achieving optimal absorption and distribution profiles.

Aqueous solubility (logS) is one of the most critical factors influencing a compound's bioavailability. Based on the ESOL model, which integrates both LogP and TPSA, compounds **9a/9b** and **10a/10b** exhibited logS values of approximately −2.60 and −2.85, respectively, classifying them as "soluble in water." In contrast, compounds **11a/11b** and **12a/12b** showed lower solubility values around −4.0, falling under the "moderately soluble" category. This trend clearly demonstrates that increasing lipophilicity and aromatic character reduce aqueous solubility. Despite constant TPSA values across the series, the observed decline in solubility suggests that increased molecular planarity may diminish solubility in aqueous environments.

In terms of in silico pharmacokinetic profiles, all compounds were predicted to have high gastrointestinal (GI) absorption, indicating favorable oral bioavailability. While compounds **10a/10b, 11a/11b,** and **12a/12b** showed the ability to cross the blood–brain barrier (BBB), compound **9a/9b** did not. This difference is attributed to variations in lipophilicity and molecular characteristics and reflects the potential for central nervous system (CNS) activity. Indeed, BBB permeability is generally consistent with higher lipophilicity, lower TPSA values, and increased molecular planarity—features that support potential CNS-targeted activity. All compounds were predicted to be non-substrates of P-glycoprotein (P-gp), suggesting they are less likely to be actively effluxed from cells. This characteristic implies that they may maintain higher intracellular concentrations, which is favorable for drug efficacy.

In terms of CYP450 enzyme inhibition, significant differences were noted. While compounds **9a/9b** and **10a/10b** were predicted not to inhibit any major CYP isoforms, compound **11a/11b** showed potential to inhibit CYP2C19 and CYP3A4, and compound **12a/12b** was predicted to inhibit CYP2C9, CYP2D6, CYP2C19, and CYP3A4. These results highlight a potentially higher risk of drug–drug interactions, particularly for compound **12a/12b**, and underscore the need for careful metabolic safety evaluation. According to skin permeability (Log Kp) data, compound **11a/11b** demonstrated the highest potential for

TABLE 3 | Predicted drug similarity parameters of isoindole 9–12 obtained from ADME analysis.

Physicochemical properties				
	9a/9b	**10a/10b**	**11a/11b**	**12a/12b**
Formula	$C_{16}H_{16}N_2O_3$	$C_{17}H_{18}N_2O_3$	$C_{21}H_{18}N_2O_3$	$C_{22}H_{20}N_2O_3$
Molecular weight (g/mol)	284.31	298.34	346.38	360.41
Num. Heavy atoms	21	22	26	27
Num. arom. Heavy atoms	6	6	12	12
Fraction Csp3	0.44	0.47	0.29	0.32
Num. Rotatable bonds	1	2	2	3
Num. H-bond acceptors	4	4	4	4
Num. H-bond donors	0	0	0	0
Molar Refractivity	83.64	88.44	103.87	108.12
TPSA ($Å^2$)	58.97	58.97	58.97	58.97
Lipophilicity				
Log $P_{o/w}$ (iLOGP)	2.10	2.39–2.42	2.62–2.64	2.70–2.79
Log $P_{o/w}$ (XLOGP3)	1.36	1.73	2.92	2.86
Log $P_{o/w}$ (WLOGP)	0.67	1.06	2.24	2.09
Log $P_{o/w}$ (MLOGP)	1.59	1.83	3.19	3.15
Log $P_{o/w}$ (SILICOS-IT)	2.05	2.42	3.08	3.46
Consensus Log $P_{o/w}$	1.55–1.59	1.89	2.81	2.85–2.87
Water solubility				
Log S (ESOL)	−2.60	−2.85	−4.04	−4.01
Solubility	7.06e-01 mg/mL; 2.48 e-03 mol/L	4.22e-01 mg/mL; 1.41 e-03 mol/L	3.18e-02 mg/mL; 9.19 e-05 mol/L	3.54e-02 mg/mL; 9.84 e-05 mol/L
Class	Soluble	Soluble	Moderately soluble	Moderately soluble
Pharmacokinetics				
GI absorption	High	High	High	High
BBB permeant	No	Yes	Yes	Yes
P-gp substrate	No	No	No	No
CYP1A2 inhibitor	No	No	No	No
CYP2C19 inhibitor	No	No	Yes	Yes
CYP2C9 inhibitor	No	No	No	Yes
CYP2D6 inhibitor	No	No	No	Yes
CYP3A4 inhibitor	No	No	Yes	Yes
Log K_p (skin permeation)	−7.07 cm/s	−6.89 cm/s	−6.34 cm/s	−6.47 cm/s
Druglikeness				
Lipinski	Yes; 0 violation	Yes; 0 violation	Yes; 0 violation	Yes; 0 violation
Ghose	Yes	Yes	Yes	Yes
Veber	Yes	Yes	Yes	Yes
Egan	Yes	Yes	Yes	Yes
Muegge	Yes	Yes	Yes	Yes
Biovailability score	0.55	0.55	0.55	0.55
Medicinal chemistry				
Pains	0 alert	0 alert	0 alert	0 alert
Brenk	1 alert: Phthalimide	1 alert: Phthalimide	1 alert: Phthalimide	1 alert: Phthalimide

(Continues)

TABLE 3 | (Continued)

Physicochemical properties				
	9a/9b	**10a/10b**	**11a/11b**	**12a/12b**
Leadlikeness	Yes	Yes	Yes	No; 1 violation: MW > 350
Synthetic accessibility	3.94	4.05	4.08	4.23

transdermal penetration, with a value of −6.34 cm/s. This suggests a possible advantage for transdermal delivery applications. All compounds met the major drug-likeness filters, including Lipinski, Ghose, Veber, Egan, and Muegge rules. These filters assess oral bioavailability and drug-likeness by evaluating key physicochemical properties such as molecular weight, hydrogen bonding capacity, TPSA, and LogP. Compliance with these rules indicates strong oral drug-likeness profiles.

From a lead-likeness perspective, all compounds except **12a/12b** complied with the criterion of molecular weight under 350 g/mol. The exception of **12a/12b** suggests that it may require structural optimization to serve as a viable lead compound. All compounds received one Brenk alert due to the presence of a phthalimide moiety, a structural feature associated with potential genotoxicity. Although no PAINS (Pan-Assay Interference Compounds) alerts were triggered—supporting the reliability of the observed bioactivities—the Brenk alert calls for further experimental validation or structural refinement to ensure safety.

Lastly, synthetic accessibility (SA) scores ranged from 3.94 for **9a/9b** to 4.23 for **12a/12b**. These values reflect moderate synthetic complexity, consistent with the addition of aromatic systems and increased molecular rigidity. Nevertheless, none of the compounds were classified as synthetically inaccessible, which supports their feasibility for laboratory synthesis and further derivatization in drug development efforts.

The obtained data indicate that as the compound series progresses structurally, lipophilicity, blood-brain barrier (BBB) permeability, and protein binding potential increase, while solubility and metabolic safety decline. Notably, compounds **10a/10b** stand out due to their balanced lipophilicity, good solubility, high gastrointestinal (GI) absorption, and favorable metabolic safety profile. In contrast, compound **12a/12b** exhibits a profile prone to potential drug–drug interactions and bioavailability issues due to its high lipophilicity and multiple CYP enzyme inhibitions. Based on these evaluations, compound **10a/10b** can be considered a lead candidate for pharmaceutical development, whereas structural optimization is recommended for compound **12a/12b**.

3.5 | BOILED-Egg Model

The BOILED-Egg model is a fast and visual computational tool used to predict the gastrointestinal (GI) absorption potential and blood-brain barrier (BBB) permeability of small molecules [56]. In this context: The white region indicates that a molecule is likely to have good GI absorption. The yellow region signifies that a molecule has the ability to cross the BBB. The gray area is reserved for molecules with low GI absorption and low brain penetration [77]. The plot displays the distribution of molecules based on two key parameters: WLOGP (lipophilicity) on one axis and TPSA (topological polar surface area) on the other. This allows a straightforward visualization of which compounds are expected to be well-absorbed orally and which have the potential to penetrate the central nervous system.

According to the in silico BOILED-Egg predictions, compounds **10–12** are located within the yellow region, indicating their potential to cross the blood-brain barrier (BBB). This suggests that these molecules could be considered potential neuroactive agents capable of exerting effects on the central nervous system (CNS). In contrast, compound **9** is located in the white region of the BOILED-Egg model, indicating a high gastrointestinal (GI) absorption potential. This suggests that compound **9** may exhibit favorable oral bioavailability. Therefore, it could be considered a more suitable candidate for therapeutic applications where systemic exposure is desired without central nervous system involvement, such as peripheral anti-inflammatory or antibacterial treatments (Scheme 3).

The optimum range for physicochemical properties (saturation, size, lipophilicity, polarity, flexibility, and solubility) are shown in the pink area on Bioavailability radars. Scheme 4 depicts the bioavailability radar for all compounds.

Scheme 4 displays the bioavailability radar plots for the synthesized compounds (**9–12**). The shaded pink area delineates the desirable range for six key parameters: lipophilicity (Lipo), molecular weight (Size), topological polar surface area (Polar), water insolubility (Insolu), degree of unsaturation (Insatu), and molecular flexibility (Flex). Furthermore, this investigation encompassed a comprehensive evaluation of the compounds' physicochemical attributes, including their lipophilicity, aqueous solubility, pharmacokinetic behavior, drug-likeness potential, and toxicity profiles.

When the docking scores and K_i values were examined, significant differences were observed in the binding capacities of the compounds to the enzymes. Since the docking score is negative, lower values indicate stronger binding. The lower the K_i value, the stronger the binding affinity of the inhibitor to the enzyme [70]. When the binding affinities to human carbonic anhydrase I were evaluated, the compounds showing the strongest binding according to docking scores were ranked as follows: **11a** (−7.62 kcal mol^{-1}) > **12a** (−7.40 kcal mol^{-1}) > **9a** (−6.90 kcal mol^{-1}) > **10a** (−6.75 kcal mol^{-1}) > **AZA** (−6.12 kcal mol^{-1}).

When the K_i values indicating inhibitory activity were analyzed, the compounds with the lowest K_i values were **11a** (23.17 ± 6.55 μM)

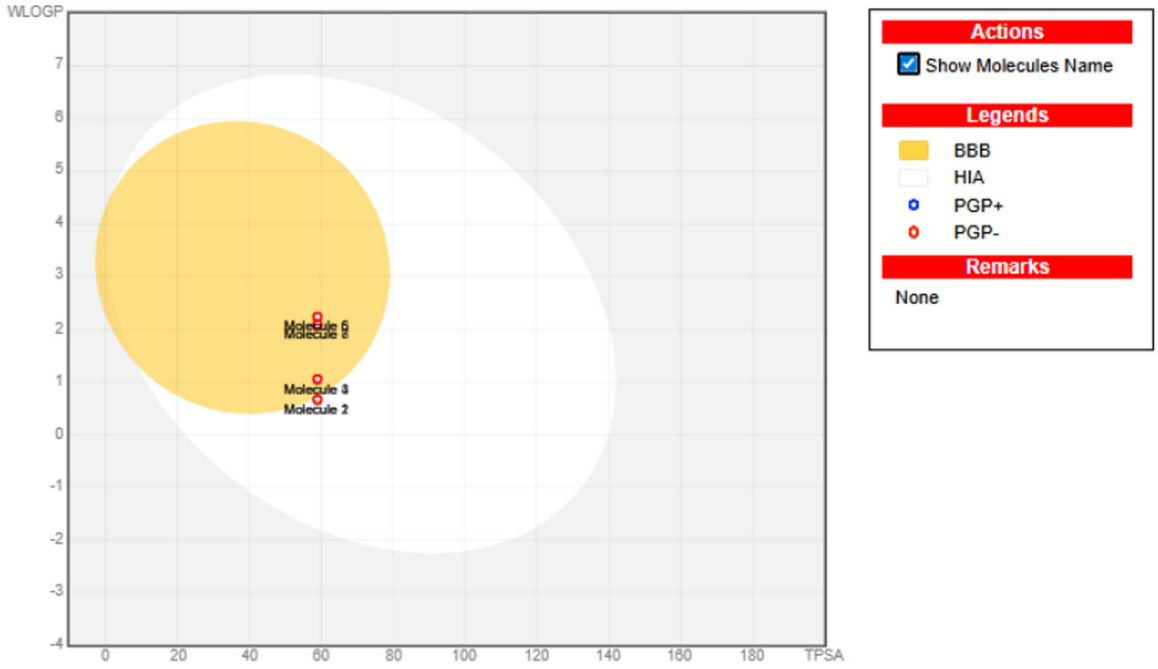

SCHEME 3 | BOILED-Egg model of compounds **9–12**.

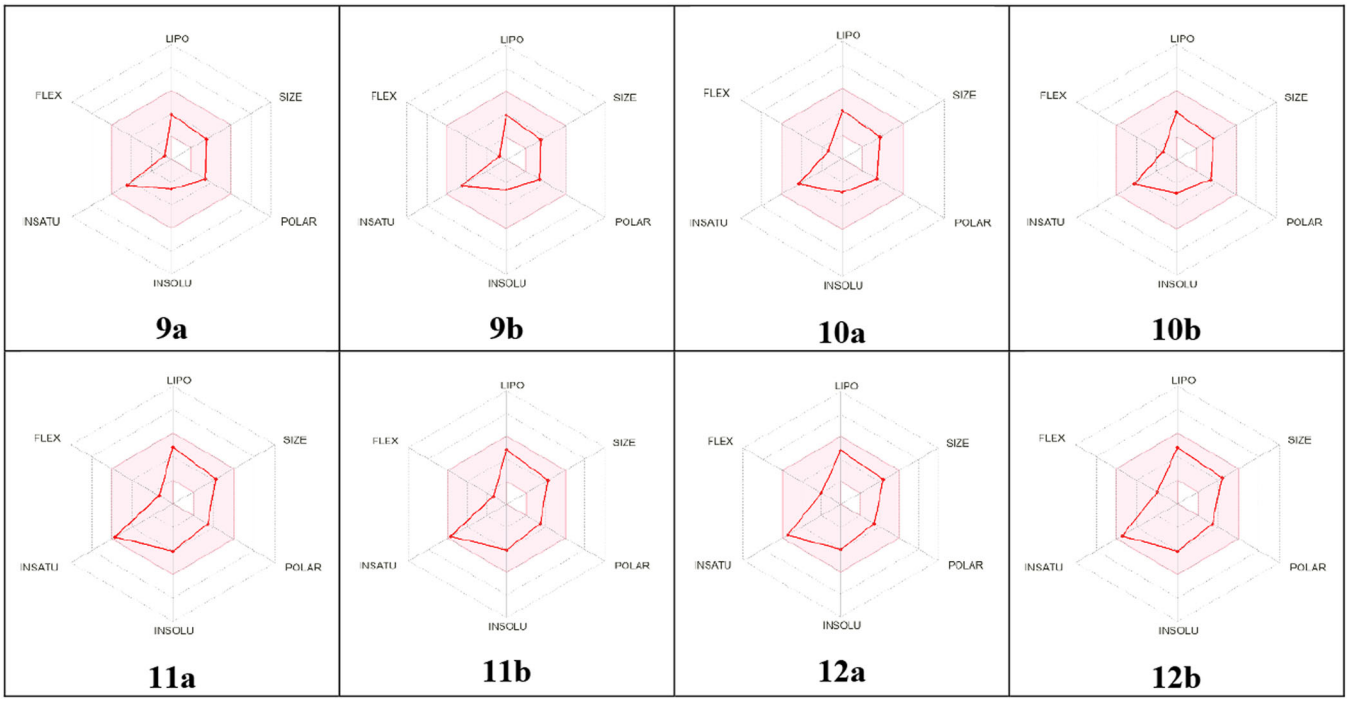

SCHEME 4 | Bioavailability radars of all synthesized compounds (**9–12**).

and **11b** ($28.52 \pm 10.85\ \mu M$). The compounds with the highest K_i values were recorded as **9a** ($79.58 \pm 13.99\ \mu M$) > **9b** ($60.63 \pm 12.64\ \mu M$) > **10b** ($48.31 \pm 5.70\ \mu M$) > **12a** ($37.45 \pm 9.85\ \mu M$) > **12b** ($31.45 \pm 8.50\ \mu M$) > **10a** ($31.10 \pm 3.14\ \mu M$). Notably, compound **11a** is one of the strongest inhibitor candidates, as it not only has the lowest docking score but also a low K_i value ($23.17 \pm 6.55\ \mu M$). On the other hand, although compound **12a** exhibits a relatively low docking score ($-7.40\ kcal\ mol^{-1}$), it has a relatively high K_i value ($37.45 \pm 9.85\ \mu M$). This indicates that a moderate concentration is required for enzyme inhibition, suggesting that its inhibitory activity is relatively weak.

When the binding affinities to human carbonic anhydrase II were assessed, the strongest binders according to docking scores were ranked as **11a** ($-7.31\ kcal\ mol^{-1}$) > **12a** ($-7.25\ kcal\ mol^{-1}$) > **9a** ($-6.86\ kcal\ mol^{-1}$) > **10a** ($-6.82\ kcal\ mol^{-1}$) > **AZA** ($-6.24\ kcal\ mol^{-1}$). When the K_i values were examined, the compounds with the lowest K_i values were determined as **10a**

(36.58 ± 6.67 μM), **11a** (37.05 ± 10.55 μM), **12b** (40.17 ± 5.11 μM), **9b** (41.22 ± 8.84 μM), and **9a** (42.60 ± 10.03 μM). Conversely, the compounds with the highest K_i values were **10b** (88.28 ± 10.22 μM), **12a** (75.81 ± 11.46 μM), and **11b** (67.07 ± 8.93 μM). Particularly, compound **11a** is considered one of the most potent inhibitor candidates, as it has both the lowest docking score (−7.31 kcal mol^{-1}) and a relatively low K_i value (37.05 ± 10.55 μM). In contrast, although compound **12a** has a low docking score (−7.25 kcal mol^{-1}), it shows a high K_i value (75.81 ± 11.46 μM). This finding indicates that a relatively high inhibitor concentration is required for enzyme inhibition, meaning that its inhibitory potency is weak. The discrepancy observed for compound **12a** suggests that, although it theoretically has favorable binding potential according to docking data, it may fail to effectively inhibit the enzyme under experimental conditions. This is known to be caused by factors such as an inappropriate binding region, conformational changes, or insufficient stabilizing interactions with the enzyme surface [29]. Moreover, docking calculations typically do not account for water molecules. However, the flexibility of the enzyme in its actual biological environment and its interactions with water molecules can affect inhibitory activity. Therefore, even if compound **12a** binds strongly to the enzyme, it may be displaced by water molecules in the biological environment or fail to remain stable due to weak interactions [29].

When the binding affinities calculated against the AChE enzyme were analyzed, compound **12a** showed the strongest binding (−10.49 kcal mol^{-1}). This was followed by **11a** (−9.58 kcal mol^{-1}), **10a** (−9.18 kcal mol^{-1}), and **9a** (−8.99 kcal mol^{-1}). The reference inhibitor tacrine exhibited the lowest binding affinity (−7.04 kcal mol^{-1}). These results reveal that all synthesized compounds have a higher binding potential to the AChE enzyme than tacrine and could therefore be considered stronger inhibitor candidates. The compounds with the lowest K_i values, and thus the strongest inhibitors, were **9a** (1.85 ± 0.18 μM) and **10a** (1.94 ± 0.53 μM). Conversely, the compound with the highest KI value and one of the weakest inhibitors was **12a** (4.02 ± 0.88 μM). Interestingly, despite having the best docking score (−10.49 kcal mol^{-1}), compound **12a** displayed a high K_i value (4.02 ± 0.88 μM). This suggests that, although the compound binds strongly to the enzyme, its inhibitory activity at the active site may be relatively low.

The docking score reflects the compound's affinity for the enzyme's binding site, whereas the KI value represents its inhibition capacity [29]. In this context, although compound **12a** has a low docking score (indicating high binding affinity), its high K_i value suggests that it binds tightly to the enzyme but exerts only limited inhibitory activity at the active site. In contrast, compounds **10a** and **11a**, which display both high docking scores and low K_i values, are among the strongest inhibitor candidates.

4 | Conclusion

In this study, a series of hexahydro-5H-isoxazolo[4,5-f]isoindole-5,7(6H)-dione derivatives were successfully synthesized via a 1,3-dipolar cycloaddition reaction, yielding both syn- and *anti*-isomers depending on the structure of the bicyclic imide precursor. The inhibitory effects of these compounds were comprehensively evaluated against human carbonic anhydrase isoenzymes (hCA I and hCA II) and AChE. Additionally, molecular docking and ADME studies were performed to further assess their therapeutic potential.

A combined evaluation of docking scores and experimental Ki values indicates that compounds **10a** and **11a** are the most promising dual inhibitors among the synthesized derivatives. In particular, compound **11a** exhibited the lowest docking scores and low K_i values (23.17 and 37.05 nM) for both hCA I and hCA II, confirming its strong theoretical binding affinity and experimental inhibitory potency. Furthermore, compound 10a exhibited both strong binding to target enzymes and effective inhibition with low KI values. Furthermore, according to IC_{50} and K_i values, all tested compounds exhibited the most potent inhibitory activities against AChE. Compounds **9a, 9b,** and **10b** exhibited low K_i values (1.85, 1.89, and 1.48 nM, respectively), indicating high inhibitory potential against AChE. The molecular docking results are consistent with the experimental data. The binding energy of tacrine, used as the reference AChE inhibitor, was calculated as −7.04 kcal/mol, and most of the synthesized compounds showed stronger binding affinities than tacrine. Similarly, compound **11a** showed the highest binding affinity to hCA I (1AZM) and hCA II (5AML) with binding energies of −7.62 and −7.31 kcal/mol, respectively. ADME analysis revealed that these compounds have favorable pharmacokinetic profiles, supporting their potential as orally bioavailable drug candidates. In particular, compound **11a** showed significant inhibition against both carbonic anhydrase isoforms and AChE, highlighting its potential as a multitarget inhibitor. These isoxazole derivatives (**9–12**), with high binding affinity, low K_i values, and favorable pharmacokinetic profiles, may serve as valuable lead molecules in the development of new therapeutic agents targeting complex disorders such as Alzheimer's disease, epilepsy, glaucoma, edema, and acute mountain sickness.

Author Contributions

Özlem Gündoğdu Aytaç: investigation, writing – review and editing, visualization, resources. **Hilal Başak Gündoğdu:** investigation, formal analysis. **Sertan Aytaç:** investigation, writing – review and editing, resources, visualization. **Zeynebe Bingöl:** investigation, visualization. **İlhami Gülçin:** conceptualization, writing – review and editing, resources. **Yunus Kara:** conceptualization, writing – original draft, resources.

Acknowledgments

The authors are appreciative to Department of Chemistry and Atatürk University for financial support.

Conflicts of Interest

The authors declare no conflicts of interest.

Data Availability Statement

The data underlying this study are available in the published article and its Supporting Information.

References

1. F. V. B. Mota, M. S. de Araújo Neta, E. de Souza Franco, et al., "Evaluation of Anti-Inflammatory Activity and Molecular Docking Study of New Aza-Bicyclic Isoxazoline Acylhydrazone Derivatives," *MedChemComm* 10 (2019): 1916–1925.

2. G. C. Arya, K. Kaur, and V. Jaitak, "Isoxazole Derivatives as Anticancer Agent: A Review on Synthetic Strategies, Mechanism of Action and SAR Studies," *European Journal of Medicinal Chemistry* 221 (2021): 113511, https://doi.org/10.1016/j.ejmech.2021.113511.

3. T. Zhang, M. Dong, J. Zhao, X. Zhang, and X. Mei, "Synthesis and Antifungal Activity of Novel Pyrazolines and Isoxazolines Derived From Cuminaldehyde," *Journal of Pesticide Science* 44 (2019): 181–185, https://doi.org/10.1584/jpestics.D19-028.

4. M. Aarjane, S. Slassi, A. Ghaleb, B. Tazi, and A. Amine, "Synthesis, Biological Evaluation, Molecular Docking and In Silico ADMET Screening Studies of Novel Isoxazoline Derivatives From Acridone," *Arabian Journal of Chemistry* 14 (2021): 103057.

5. V. V. Pothuri, P. V. S. Machiraju, and V. S. S. Rao, "Synthesis and Biological Activity of Some Novel Derivatives of 4-[5-(2,3-Dihydrobenzo [b][1,4]Dioxin-7-yl)Isoxazole-3-yl]Benzoic Acid," *Russian Journal of General Chemistry* 90 (2020): 889–894.

6. C. Dallanoce, G. Meroni, M. De Amici, C. Hoffmann, K. N. Klotz, and C. De Micheli, "Synthesis of Enantiopure Δ2-isoxazoline Derivatives and Evaluation of Their Affinity and Efficacy Profiles at Human β-Adrenergic Receptor Subtypes," *Bioorganic & Medicinal Chemistry* 14 (2006): 4393–4401.

7. E. Ghidini, A. M. Capelli, C. Carnini, et al., "Discovery of a Novel Isoxazoline Derivative of Prednisolone Endowed With a Robust Anti-Inflammatory Profile and Suitable for Topical Pulmonary Administration," *Steroids* 95 (2015): 88–95.

8. M. Ahmed, M. A. Qadir, A. Hameed, M. Imran, and M. Muddassar, "Screening of Curcumin-Derived Isoxazole, Pyrazoles, and Pyrimidines for Their Anti-Inflammatory, Anti-nociceptive, and cyclooxygenase-2 Inhibition," *Chemical Biology & Drug Design* 91 (2018): 338–343.

9. D. Goyard, B. Kónya, A. S. Chajistamatiou, et al., "Glucose-Derived Spiro-Isoxazolines Are Anti-Hyperglycemic Agents Against Type 2 Diabetes Through Glycogen Phosphorylase Inhibition," *European Journal of Medicinal Chemistry* 108 (2016): 444–454.

10. S. Fettach, F. Z. Thari, Z. Hafidi, et al., "Biological, Toxicological, and Molecular Docking Evaluations of Isoxazoline-Thiazolidine-2,4-Dione Analogues as a New Class of Anti-Hyperglycemic Agents," *Journal of Biomolecular Structure and Dynamics* 12 (2021): 1072–1084.

11. A. Galbiati, A. Zana, C. Coser, et al., "Development of Potent 3-Br-Isoxazoline-Based Antimalarial and Antileishmanial Compounds," *ACS Medicinal Chemistry Letters* 12 (2021): 1726–1732.

12. A. Phanumartwiwath, C. Kesornpun, S. Sureram, et al., "Antitubercular and Antibacterial Activities of Isoxazolines Derived From Natural Products: Isoxazolines as Inhibitors of *Mycobacterium tuberculosis* InhA," *Journal of Chemical Research* 45 (2021): 1003–1015.

13. J. R. Pruitt, D. J. Pinto, M. J. Estrella, et al., "Isoxazolines and Isoxazoles as Factor Xa Inhibitors," *Bioorganic & Medicinal Chemistry Letters* 10 (2000): 685–689.

14. M. Güney, A. Coşkun, F. Topal, A. Daştan, İ. Gülçin, and C. T. Supuran, "Oxidation of Cyanobenzocycloheptatrienes: Synthesis, Photooxygenation Reaction and Carbonic Anhydrase Isoenzymes Inhibition Properties of Some New Benzotropone Derivatives," *Bioorganic & Medicinal Chemistry* 22, no. 13 (2014): 3537–3543.

15. Ç. Bayrak, P. Taslimi, İ. Gülçin, and A. Menzek, "The First Synthesis of 4-Phenylbutenone Derivative Bromophenols Including Natural Products and Their Inhibition Profiles for Carbonic Anhydrase, Acetylcholinesterase, and Butyrylcholinesterase Enzymes," *Bioorganic Chemistry* 72 (2017): 359–366.

16. M. Nar, Y. Çetinkaya, İ. Gülçin, and A. Menzek, "(3,4-Dihydroxyphenyl)(2,3,4-trihydroxyphenyl)methanone and Its Derivatives as Carbonic Anhydrase Isoenzymes Inhibitors," *Journal of Enzyme Inhibition and Medicinal Chemistry* 28, no. 2 (2013): 402–406.

17. B. Turan, K. Şendil, E. Şengül, et al., "The Synthesis of Some β-Lactams and Investigation of Their Metal Chelating Activity, Carbonic Anhydrase and Acetylcholinesterase Inhibition Profiles," *Journal of Enzyme Inhibition and Medicinal Chemistry* 31, no. S1 (2016): 79–88.

18. Y. Akbaba, A. Akıncıoğlu, H. Göçer, S. Göksu, İ. Gülçin, and C. T. Supuran, "Carbonic Anhydrase Inhibitory Properties of Novel Sulfonamide Derivatives of Aminoindanes and Aminotetralins," *Journal of Enzyme Inhibition and Medicinal Chemistry* 29, no. 1 (2014): 35–42.

19. P. Taslimi, İ. Gülçin, N. Öztaşkın, et al., "The Effects of Some Bromophenols on Human Carbonic Anhydrase Isoenzymes," *Journal of Enzyme Inhibition and Medicinal Chemistry* 31, no. 4 (2016): 603–607.

20. C. T. Supuran, "Carbonic Anhydrases: Novel Therapeutic Applications for Inhibitors and Activators," *Nature Reviews Drug Discovery* 7 (2008): 168–181.

21. F. Ozbey, P. Taslimi, İ. Gülçin, A. Maraş, S. Goksu, and C. T. Supuran, "Synthesis, Acetylcholinesterase, Butyrilcholinesterase, Carbonic Anhydrase Inhibitory and Metal Chelating Properties of Some Novel Diaryl Ether," *Journal of Enzyme Inhibition and Medicinal Chemistry* 31, no. S2 (2016): 79–85.

22. A. J. Kivelä, "Carbonic Anhydrases in Normal Gastrointestinal Tract and Gastrointestinal Tumours," *World Journal of Gastroenterology* 11, no. 2 (2005): 155–163.

23. S. Mert, Y. Demir, Y. Sert, R. Kasımoğulları, and İ. Gülçin, "Synthesis, Biological Evaluation and Molecular Docking of Novel Pyrazole Derivatives as Multitarget Acetylcholinesterase and Carbonic Anhydrase Inhibitors," *Journal of Molecular Structure* 1319, no. 5 (2025): 139472.

24. L. Durmaz, H. Karageçili, A. Erturk, et al., "Hamamelitannin's Antioxidant Effect and Its Inhibition Capability on α-Glycosidase, Carbonic Anhydrase, Acetylcholinesterase, and Butyrylcholinesterase Enzymes," *Processes* 12, no. 11 (2024): 2341.

25. E. D. Dincel, F. Başoğlu-Ünal, E. D. Kuran, et al., "Design, Synthesis, and Evaluation of Novel Bistrifluoromethyl-Based Hydrazones as Dual Inhibitors of Acetylcholinesterase and Carbonic Anhydrase Enzymes for Alzheimer's Disease," *Chemical Biology & Drug Design* 103, no. 2 (2024): 4482.

26. D. A. Annan, N. Maishi, T. Soga, et al., "Carbonic Anhydrase 2 (CAII) Supports Tumor Blood Endothelial Cell Survival Under Lactic Acidosis in the Tumor Microenvironment," *Cell Communication and Signaling* 17 (2019): 169.

27. P. Taslimi, E. Koksal, A. C. Gören, et al., "Anti-Alzheimer, Antidiabetic and Antioxidant Potential of *Satureja cuneifolia* and Analysis of Its Phenolic Contents by LC-MS/MS," *Arabian Journal of Chemistry* 13, no. 3 (2020): 4528–4537.

28. M. Yıldırım, H. Ünver, A. Necip, and M. Çimentepe, "Design, Synthesis, and Biological Evaluation of Novel Vanillin-Derived Hydrazone Compounds With Antimicrobial, Anticancer, and Enzyme Inhibition Activities, Along With Molecular Structure and Drug-Likeness Assessment," *Biochemical and Biophysical Research Communications* 775 (2025): 152173.

29. A. Karakaya, U. Acar Çevik, B. Kaya, et al., "Design, Synthesis, In Silico Absorption, Distribution, Metabolism, and Elimination and Molecular Docking Studies of Thiazole-Based Furan Derivatives, and Their Biological Evaluation for Alzheimer Disease Therapy," *ChemistryOpen* 2025): e202500305, https://doi.org/10.1002/open.202500305.

30. C. Yamali, H. I. Gul, C. Kazaz, and S. Levent, "İ. Gülçin, "Synthesis, Structure Elucidation, and In Vitro Pharmacological Evaluation of Novel Polyfluoro Substituted Pyrazoline Type Sulfonamides as Multi-Target Agents for Inhibition of Acetylcholinesterase and Carbonic Anhydrase I and II Enzymes," *Bioorganic Chemistry* 96 (2020): 103627.

31. S. Bal, R. Kaya, Y. Gök, et al., "Novel 2-Methylimidazolium Salts: Synthesis, Characterization, Molecular Docking, and Carbonic Anhydrase and Acetylcholinesterase Inhibitory Properties," *Bioorganic Chemistry* 94 (2020): 103468.

32. A. Bytyqi-Damoni, A. Kestane, P. Taslimi, et al., "Novel Carvacrol-Based New Oxypropanolamine Derivatives: Design, Synthesis, Characterization, Biological Evaluation, and Molecular Docking Studies," *Journal of Molecular Structure* 1202 (2020): 127297.

33. I. Demirhan, A. Necip, E. Oner, et al., "Imidazolium Salts Carrying Two Positive Charges: Design, Synthesis, Characterization, Molecular Docking, Antibacterial and Enzyme Inhibitory Activities," *Frontiers in Cellular and Infection Microbiology* 15 (2025).

34. E. Yetişkin, Ö. Gündoğdu, D. Mete, N. Çelebioğlu, Y. Kara, and G. Şanlı-Mohamed, "Synthesis, Cytotoxicity, and Antibacterial Studies of 2,4,5,6-substituted Hexahydro-1H-Isoindole-1,3(2H)-Dione," *Chemical Biology & Drug Design* 102, no. 6 (2023): 1448–1457.

35. A. K. Süloğlu, G. Selmanoğlu, Ö. Gündoğdu, et al., "Evaluation of Isoindole Derivatives: Antioxidant Potential and Cytotoxicity in the HT-29 Colon Cancer Cells," *Archiv der Pharmazie* 353, no. 11 (2020): 2000065.

36. A. Tan, B. Koc, E. Sahin, N. H. Kishali, and Y. Kara, "Synthesis of New Cantharimide Analogues Derived From 3-Sulfolene," *Synthesis* 4 (2011): 1079–1084.

37. A. Tan, M. Z. Kazancioğlu, D. Aktaş, et al., "Convenient Synthesis of New Polysubstituted Isoindole-1,3-Dione Analogues," *Turkish Journal of Chemistry* 38 (2014): 629–637.

38. Ö. Gündoğdu, A. Atalay, N. Çelebioğlu, et al., "Regio- and Stereochemical Ring-Opening Reactions of the 2,3-Epoxy Alcohol Derivative With Nucleophiles: Explanation of the Structures and C-2 Selectivity Supported by Theoretical Computations," *Journal of Molecular Structure* 1264 (2022): 133163.

39. Ö. G. Aytaç, E. N. Özkan, Y. Kara, and E. Şahin, "Synthesis, Structural Studies, and Hirshfeld Surface Analysis of the Substituted Isoindole-1,3-Dione Derivatives," *Journal of Molecular Structure* 1321 (2025): 140204.

40. Ö. Gündoğdu, A. Atalay, P. Turhan, et al., "Reduction of 2-Phenyl-3a,4,7,7a-Tetrahydro-1H-Isoindole-1,3(2H)-Dione With $NaBH_4$: Investigation of Exo-Selectivity and Reaction Mechanism via Theoretical Computations,," *Journal of Molecular Structure* 1319, no. 1 (2025): 139520.

41. A. Beycet, P. Taslimi, B. Şen, et al., "New Palladium Complexes With N-Heterocyclic Carbene and Morpholine Ligands: Synthesis, Characterization, Crystal Structure, Molecular Docking, and Biological Activities," *Biochemical and Molecular Toxicology* 38, no. 1 (2024): e23554.

42. R. E. Bora, H. Genc Bilgicli, E. M. Üç, M. A. Alagöz, M. Zengin, and İ. Gulcin, "Synthesis, Characterization, Evaluation of Metabolic Enzyme Inhibitors, and in Silico Studies of Thymol-Based 2-Amino Thiol and Sulfonic Acid Compounds," *Chemico-Biological Interactions* 366 (2022): 110134.

43. J. A. Verpoorte, S. Mehta, and J. T. Edsall, "Esterase Activities of Human Carbonic Anhydrases B and C," *Journal of Biological Chemistry* 242 (1967): 4221–4229.

44. M. M. Bradford, "A Rapid and Sensitive Method for the Quantitation of Microgram Quantities of Protein Utilizing the Principle of Protein-Dye Binding," *Analytical Biochemistry* 72 (1976): 248–254.

45. U. K. Laemmli, "Cleavage of Structural Proteins During the Assembly of the Head of Bacteriophage T4," *Nature* 227 (1970): 680–685.

46. A. Karimov, A. Orujova, P. Taslimi, et al., "Novel Functionally Substituted Esters Based on Sodium Diethyldithiocarbamate Derivatives: Synthesis, Characterization, Biological Activity and Molecular Docking Studies," *Bioorganic Chemistry* 99 (2020): 103762.

47. H. Lineweaver and D. Burk, "The Determination of Enzyme Dissociation Constants," *Journal of the American Chemical Society* 56 (1934): 658–666.

48. Ö. Gündoğdu, "'Molecular Docking Studies and ADME Predictions on Synthesized Chalcone Compounds Targeting EGFR,' Hittite," *Journal of Science and Engineering* 10, no. 2 (2023): 167–175.

49. I. T. Babalola and G. Suleiman, "Design, Synthesis, and Molecular Docking Studies of N-Substituted Sulfonamides as Potential Anticancer Therapeutics," *Journal of Taibah University Medical Sciences* 19 (2024): 175–183.

50. R. Zengin, Y. Gök, Y. Demir, et al., "Fluorinated Benzimidazolium Salts: Synthesis, Characterization, Molecular Docking Studies and Inhibitory Properties Against Some Metabolic Enzymes," *Journal of Fluorine Chemistry* 267 (2023): 110094.

51. J. Ivanova, J. Leitans, M. Tanc, et al., "X-Ray Crystallography-Promoted Drug Design of Carbonic Anhydrase Inhibitors," *Chemical Communications* 51 (2015): 7108–7111.

52. I. Mahmudov, Y. Demir, Y. Sert, et al., "Synthesis and Inhibition Profiles of N-Benzyl- and N-Allyl Aniline Derivatives Against Carbonic Anhydrase and Acetylcholinesterase—A Molecular Docking Study," *Arabian Journal of Chemistry* 15, no. 3 (2022): 103645.

53. E. Güzel, Ü. M. Koçyiğit, P. Taslimi, et al., "Phthalocyanine Complexes With (4-Isopropylbenzyl)oxy Substituents: Preparation and Evaluation of Anti-Carbonic Anhydrase, Anticholinesterase Enzymes and Molecular Docking Studies," *Journal of Biomolecular Structure and Dynamics* 40 (2022): 733–741.

54. H. Yakan, Ü. M. Koçyiğit, H. Muğlu, et al., "Potential Thiosemicarbazone-Based Enzyme Inhibitors: Assessment of Anti-proliferative Activity, Metabolic Enzyme Inhibition Properties, and Molecular Docking Calculations," *Journal of Biochemical and Molecular Toxicology* 36, no. 5 (2022): e23018.

55. G. Xiong, Z. Wu, J. Yi, et al., "ADMETlab 2.0: An Integrated Online Platform for Accurate and Comprehensive Predictions of ADMET Properties," *Nucleic Acids Research* 49, no. W1 (2021): W5–W14.

56. A. Daina, O. Michielin, and V. Zoete, "SwissADME: A Free Web Tool to Evaluate Pharmacokinetics, Drug-Likeness and Medicinal Chemistry Friendliness of Small Molecules," *Scientific Reports* 7 (2017): 42717.

57. A. Santu and E. Manoj, "Coumarin Based Schiff Base Proligands as Promising Antioxidant, Antibacterial and Anticancer Agents: DFT and Molecular Docking Correlations," *Journal of Molecular Structure* 1333 (2025): 141650.

58. T. Morita, S. Yugandar, S. Fuse, and H. Nakamura, "Recent Progresses in the Synthesis of Functionalized Isoxazoles," *Tetrahedron Letters* 59, no. 13 (2018): 1159–1171.

59. M. I. Hossain, M. I. H. Khan, S. J. Kim, and H. V. Le, "Synthesis of 3,4,5-Trisubstituted Isoxazoles in Water via a [3 + 2]-Cycloaddition of Nitrile Oxides and 1,3-Diketones, β-Ketoesters, or B-Ketoamides," *Beilstein Journal of Organic Chemistry* 18 (2022): 446–458.

60. S. Das and K. Chanda, "An Overview of Metal-Free Synthetic Routes to Isoxazoles: The Privileged Scaffold," *RSC Advances* 11 (2021): 32680–32705.

61. A. Kumar and P. Jayaroopa, "Isoxazoles: Molecules With Potential Medicinal Properties," *IJPBS* 3, no. 2 (2013): 294–304.

62. N. C. Tran, H. Dhondt, M. Flipo, B. Deprez, and N. Willand, "Synthesis of Functionalized 2-Isoxazolines as Three-Dimensional Fragments for Fragment-Based Drug Discovery," *Tetrahedron Letters* 56 (2015): 4119–4123.

63. A. S. El-Azab, A. A. M. Abdel-Aziz, H. A. Ghabbour, et al., "Carbonic Anhydrase Inhibition Activities of Schiff's Bases Based on Quinazoline-Linked Benzenesulfonamide," *Molecules* 27, no. 22 (2022): 7703.

64. S. Hashmi, S. Khan, Z. Shafiq, et al., "Probing 4-(Diethylamino)-Salicylaldehyde-Based Thiosemicarbazones as Multi-Target Directed Ligands Against Cholinesterases, Carbonic Anhydrases and α-Glycosidase Enzymes," *Bioorganic Chemistry* 107 (2021): 104554.

65. D. Meier, T. H. Collet, I. Locatelli, et al., "Does This Patient Have Acute Mountain Sickness: The Rational Clinical Examination Systematic Review," *Journal of the American Medical Association* 318 (2017): 1810–1819.

66. Y. Kaya, A. Erçağ, Y. Zorlu, Y. Demir, and İ. Gülçin, "New Pd(II) Complexes of the Bisthiocarbohydrazones Derived From Isatin and Disubstituted Salicylaldehydes: Synthesis, Characterization, Crystal Structures and Inhibitory Properties Against Some Metabolic Enzymes," *JBIC, Journal of Biological Inorganic Chemistry* 27, no. 2 (2022): 271–281.

67. A. Aktas, D. Barut Celepci, Y. Gok, P. Taslimi, H. Akincioglu, and İ. Gulcin, "A Novel Ag-N-Heterocyclic Carbene Complex Bearing the Hydroxyethyl Ligand: Synthesis, Characterization, Crystal and Spectral Structures and Bioactivity Properties," *Crystals* 10 (2020): 171.

68. S. Aytac, O. Gundogdu, Z. Bingol, and İ. Gulcin, "Synthesis of Schiff Bases Containing Phenol Rings and Investigation of Their Antioxidant Capacity, Anticholinesterase, Butyrylcholinesterase, and Carbonic Anhydrase Inhibition Properties,," *Pharmaceutics* 15, no. 3 (2023): 779.

69. G. L. Ellman, K. D. Courtney, V. Andres, and R. M. Feather-Stone, ""A New and Rapid Colorimetric Determination of Acetylcholinesterase Activity," *Biochemical Pharmacology* 7, no. 2 (1961): 88–95.

70. M. Yildirim, K. Dogan, A. Necip, and M. Cimentepe, "Naringenin-Loaded Phema Cryogel Membrane: Preparation, Characterization, Antibacterial Activity and In Silico Studies," *Chemical Papers* 79 (2025): 211–220.

71. F. S. Tokalı, P. Taslimi, B. Tüzün, A. Karakuş, N. Sadeghian, and İ. Gulçin, "Synthesis of New Carboxylates and Sulfonates Containing Thiazolidin-4-One Ring and Evaluation of Inhibitory Properties Against Some Metabolic Enzymes," *Journal of the Iranian Chemical Society* 20, no. 10 (2023): 2631–2642.

72. N. Saini, A. S. Grewal, V. Lather, and S. K. Gahlawat, "Natural Alkaloids Targeting EGFR in Non-Small Cell Lung Cancer: Molecular Docking and ADMET Predictions," *Chemico-Biological Interactions* 358 (2022): 109901.

73. R. G. Tatar and B. S. Kurşun Aktar, "Bazı Kalkonların COVID−19 Tedavisine Yönelik SARS-CoV-2 Ana Proteaza Bağlanma Mekanizmasının Moleküler Kenetleme Yaklaşımı Ile Aydınlatılması [Elucidation of the Binding Mechanism of Several Chalcone Against SARS-CoV-2 Main Protease Enzyme for COVID-19 Treatment by Molecular Docking Approach]," *International Journal of Advanced Engineering and Pure Sciences* 33, no. 4 (2021): 660–669.

74. S. Alyar, Ü. Ö. Özmen, Ş. Adem, K. Erdem, and H. Alyar, "Synthesis, Molecular Docking Study, Molecular Dynamics Simulation and ADMET Prediction of New Sulfa Drugs Having CA II Inhibitory Effect and Antidiabetic Activity," *Journal of Molecular Structure* 1336 (2025): 142015.

75. B. Kaya, U. Acar Çevik, A. Necip, et al., "Design, Synthesis, Biological Evaluation, and Molecular Docking Studies of Novel 1,3,4-Thiadiazole Derivatives Targeting Both Aldose Reductase and α-Glucosidase for Diabetes Mellitus," *ACS Omega* 10 (2025): 18812–18828.

76. C. Wilson, "Lipophilicity: Understanding the Role of Lipid Affinity in Drug Design and Absorption," *Journal of Pharmacokinetics & Experimental Therapeutics* 8 (2024): 6.

77. B. Kaya, H. Tahtacı, B. Çiftçi, et al., "Discovery of Hydrazine Clubbed Thiazoles as Potential Antidiabetic Agents: Synthesis, Biological Evaluation, and Molecular Docking Studies," *Drug Development Research* 86 (2025): e70060.

Supporting Information

Additional supporting information can be found online in the Supporting Information section.
Supporting info - Revised.